Supporting Information

Covalent adaptable networks through dynamic *N,S*-acetal chemistry: toward recyclable CO_2-based thermosets

Thomas Habets[a], Guillem Seychal[b,c], Marco Caliari[a,c], Jean-Marie Raquez[b], Haritz Sardon[c], Bruno Grignard[a,d], Christophe Detrembleur[a]*

[a] Center for Education and Research on Macromolecules (CERM), CESAM Research Unit, University of Liege, Sart-Tilman B6a, 4000 Liege, Belgium

[b] Laboratory of Polymeric and Composite Materials, Center of Innovation and Research in Materials and Polymers (CIRMAP), Uni-versity of Mons UMONS, Place du Parc 20, 7000 Mons, Belgium

[c] POLYMAT, University of the Basque Country UPV/EHU, Joxe Mari Korta Center, Avda. Tolosa 7, 20018 Donostia-San Sebastian, Spain

[d] FRITCO2T Platform, University of Liege, Sart-Tilman B6a, 4000 Liege, Belgium

*Email: christophe.detrembleur@uliege.be

1. Materials and Instrumentation

Materials

Benzylamine (99%) was purchased from Sigma Aldrich.
Benzyl mercaptan (99%) was purchased from Sigma Aldrich.
2,2′-(Ethylenedioxy)diethanethiol (**DMDO**, 95%) was purchased from Sigma Aldrich.
Hexamethylenediamine (**HMDA**, 98%) was purchased from Sigma Aldrich.
Methanesulfonic acid (**MSA**, 99%) was purchased from Sigma Aldrich.
2-Methylbut-3-yn-2-ol (98%) was purchased from Sigma Aldrich.
Molecular sieves (3A, 2-5mm beads) were purchased from Thermo Scientific.
1-Octanethiol (98.5%) was purchased from Sigma Aldrich.
Pentaerythritol tetrakis(3-mercaptopropionate) (**PETMP**, 95%) was purchased from Sigma Aldrich.
Priamine 1075 (**PRI**) was kindly supplied by Croda.
Propylamine (99%) was purchased from Sigma Aldrich.
Silver carbonate (**Ag_2CO_3**, 99%) was purchased from Sigma Aldrich.
Triethylamine (99%) was purchased from Acros Organics.
Triphenylphosphine (99%) was purchased from Sigma Aldrich.
m-Xylylenediamine (**XDA**, 99%) was purchased from Sigma Aldrich.

All reagents were used as received without purification.

Instrumentation

Nuclear magnetic resonance (NMR) spectroscopy. ^{1}H- and ^{13}C-NMR analyses were performed on a Bruker 400 MHz spectrometer at 25 °C in the Fourier transform mode. 16 scans for ^{1}H spectra and 512 scans for ^{13}C spectra were recorded.
High resolution mass spectrometry (HRMS). ESI-MS data were acquired on a Waters Synapt G2-Si mass spectrometer (Waters, UK) equipped with an Electrospray ionization source used in the positive ion mode. Samples were prepared as followed, 1mg/mL solution in Acetonitrile solution were diluted 500 times to reach a final concentration of 2.10-6 g/mL. For the mass spectrometer parameters, the Electrospray ionization (ESI) conditions were capillary voltage 3.1 kV; cone voltage 30 V; source temperature 120 °C; desolvation temperature 150 °C. Dry nitrogen, the desolvation gas, is used as the ESI gas with a flow rate of 500 $L.h^{-1}$. Mass accuracy measurement (HRMS) were performed by using lock spay unit, available on the source ion block, by infusing NaI solution as reference in order to perform internal calibration.
Fourier Transform Infrared Spectra (FT-IR). FTIR measurements were carried out on a Nicolet IS5 spectrometer (Thermo Fisher Scientific) equipped with a diamond attenuated transmission reflectance (ATR) device. 32 scans were recorded for each sample over the range 4000-500 cm^{-1} with a normal resolution of 4 cm^{-1}.
Thermogravimetric analysis (TGA). TGA analysis was performed on a TGA2 instrument from Mettler Toledo. Around 5 of sample was heated at 10 °C/min from 30 to 50 °C and flushed for 10 min at 50 °C. The sample was then heated at 20 °C/min until 600 °C. All the experiment was conducted under nitrogen atmosphere (20 mL/min).
Differential scanning calorimetry (DSC). DSC analysis was performed on a DSC 250 (TA Instruments). All the experiments were performed under ultrapure nitrogen flow. Samples of 4–6 mg were used and placed in hermetic aluminum pans. The sample was cooled to -40 °C and the temperature modulated segment was set with an amplitude of 1 °C with a period of 60 seconds. The sample was then heated to 120 °C at a rate of 2 °C/min. The glass transition temperatures were determined using the reversing heat flow curve.
Rheology. Rheology experiments were conducted on an ARES G2 rheometer from TA Instruments in shear geometry with a plate diameter of 8 mm. The samples were prepared by compression molding and were cut in their rubber state using a die cutter. Temperature sweeps were performed at a rate of 2 °C/min at a frequency of 1 Hz and at a constant strain of 1%. Stress relaxation experiments were performed with a constant shear strain of 1% within the linear viscoelastic region of the polymers.

Dynamic mechanical analysis (DMA). DMA experiment was performed on a DMA Q800 from TA Instruments. Temperature ramp experiment was performed in tension mode with 0.01 N of constant force and a frequency of 1 Hz. The sample was equilibrated at 30 °C and heated with a heating rate of 2 °C/min until 80 °C.

Swelling Ratio (SR) and Gel Content (GC). The swelling ratio (SR) was determined by immersion of a piece of material (between 100 and 200 mg) of mass m_i in THF (or neutralized THF with some drops of triethylamine). After 24h, the swollen sample was weighted as the mass of the gel m_{gel}. The SR was calculated using the following equation.

$$SR\ (\%) = \frac{m_{gel} - m_i}{m_i} \times 100$$

The gel content (GC) was determined by weighting the mass m_f after drying of the swollen sample using the following equation.

$$GC\ (\%) = \frac{m_f}{m_i} \times 100$$

Tensile tests. Tensile tests were conducted at room temperature using a ZwickRoell Z2.5 at a speed of 2 $mm.min^{-1}$ or 10 $mm.min^{-1}$ (in the case of the elastomeric P-PRI). Measurements were repeated 5 times on dogbone-shaped samples (ASTM-D1708) with a thickness of around 1 mm. The samples were prepared by compression molding and were cut in their rubber state using a die cutter. For reprocessing studies represented in Figure S45, the dogbone specimens of P-DMDO were reprocessed after fracture by compression molding at 100 °C (10 min, 1 ton metric) and were cut in their rubber state using a die cutter.

Compression molding. Polymer samples were cut into little pieces and pressed in a steel mold between Teflon sheets in a Carver press. All the samples were pressed at a temperature just above their flowing transition (between 80 and 100 °C) for 10 min under 1 ton metric of pressure. The mold was then removed from the press and slowly cooled down to r.T.

Extrusion. The polymer P-HMDA was cut in little pieces and introduced in a pre-heated DSM micro compounder at 90 °C. The polymer was mixed for few minutes at 90 °C and extruded at a screw speed of 150 rpm.

Injection molding. The polymer P-HMDA was cut in little pieces and introduced in the injection chamber of the DSM Xplore Mini for 10 min at 50 °C. It was then injected at 90 °C with a pressure of around 700 bars in the mold.

2. Synthetic Procedures toward model alkylidene oxazolidones

A. Synthesis of 4,4-dimethyl-5-methylene-1,3-dioxolan-2-one (αCC)

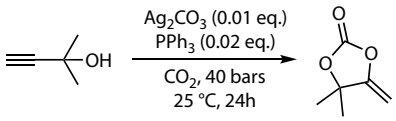

αCC was synthesized by modification of Q. Song's procedure[1]. 2-Methyl-3-butyn-2-ol (125 mL, 1.3 mol, 1 eq.), Ag_2CO_3 (3.585 g, 13 mmol, 0.01 eq.), Triphenylphosphine (6.82 g, 26 mmol, 0.02 eq.) and 20 mL of Chloroform were added in a 250 mL high pressure autoclave. The reactor was charged with 40 bars of CO_2 at 25°C. After 14h, the reactor was depressurized. The crude mixture was distilled under vacuum. The resulting transparent liquid was solubilized in 600 mL of diethyl ether and extracted with water (3 x 600 mL). The organic phase was dried over $MgSO_4$, filtered, and dried under vacuum. The pure product crystallized into a white solid (126.3 g, isolated yield 76 %); mp = 31 °C; **^{1}H NMR** (400 MHz, DMSO-d_6) δ 4.79 (d, J = 3.8 Hz, 1H), 4.65 (d, J = 3.8 Hz, 1H), 1.60 (s, 6H); **^{13}C NMR** (100 MHz, DMSO-d_6) δ 158.7, 151.3, 85.9, 85.6, 27.4.

B. Synthesis of 4-hydroxy-4,5,5-trimethyl-3-propyloxazolidin-2-one (1a)

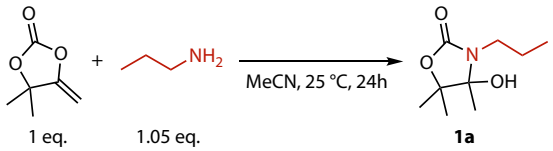

αCC (1.536 g, 12 mmol, 1 eq.), Propylamine (0.744 g, 12.6 mmol, 1.05 eq.), and acetonitrile (3 mL) were added to a round-bottom flask immerged in an ice bath. The mixture was stirred for 1h and 23h more at 25 °C. Solvent and excess amines were removed under vacuum to yield the product **1a** as white crystals (2.1 g, isolated yield 95 %); mp = 69 °C; **^{1}H NMR** (400 MHz, DMSO-d_6) δ 5.90 (s, 1H), 3.02 (m, 2H), 1.52 (sextuplet, J = 7.4 Hz, 2H), 1.29 (s, 3H), 1.28 (s, 3H), 1.22 (s, 3H), 0.85 (t, J = 7.4 Hz, 3H); **^{13}C NMR** (100 MHz, DMSO-d_6) δ 157.0, 89.7, 84.5, 41.6, 25.1, 22.8, 21.0, 20.9, 11.8.

C. Synthesis of 3-benzyl-4-hydroxy-4,5,5-trimethyloxazolidin-2-one (1b)

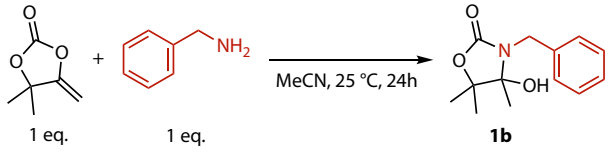

αCC (1.536 g, 12 mmol, 1 eq.), Benzylamine (1.284 g, 12 mmol, 1 eq.), and acetonitrile (3 mL) were added to a reaction tube and the mixture was stirred for 24h. The precipitate was then dissolved in more Acetonitrile (around 25 mL) and put at -20 °C overnight for recrystallization. The crystals were filtered, washed with cold diethyl ether, and dried under vacuum. The pure product **1b** was isolated as white crystals (2.48 g, isolated yield 88 %); mp = 145 °C; **^{1}H NMR** (400 MHz, DMSO-d_6) δ 7.31 (m, 5H), 6.15 (s, 1H), 4.43 (d, J = 16.2 Hz, 1H), 4.20 (d, J = 16.2 Hz, 1H), 1.32 (s, 3H), 1.26 (s, 3H), 1.12 (s, 3H); **^{13}C NMR** (100 MHz, DMSO-d_6) δ 157.5, 139.4, 128.8, 127.3, 89.8, 84.9, 43.1, 25.2, 21.2, 21.0.

D. Dehydration setup for the facile synthesis of alkylidene oxazolidone

A dehydration setup was designed to allow for quantitative dehydration of hydroxyoxazolidones **1** into **2** without the need of chromatography purification. The compound **1** was dissolved in acetonitrile and an acid catalyst (here, MSA) was added to catalyze dehydration. In order to push the reaction to full conversion, the acetonitrile forming an azeotrope with water was refluxed through an addition funnel containing molecular sieves (Figure S1). Water-free solvent is recovered during the reaction and the equilibrium can be shifted thanks to the molecular sieves acting as water scavenger. After reaction, the molecular sieves can be recovered and simply dried as there was no contact with any chemicals apart water and the solvent (here, acetonitrile).

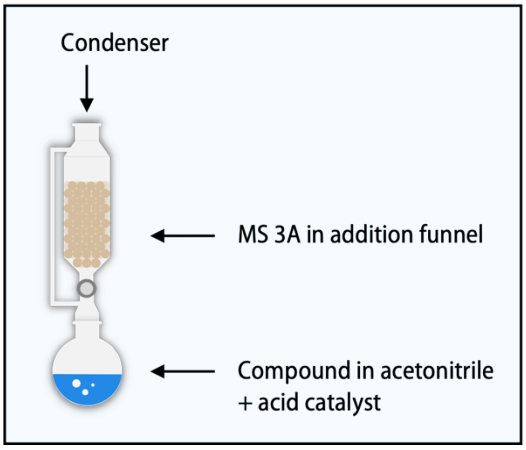

Figure S1 – Schematic representation of the dehydration setup.

E. General procedure for the synthesis of alkylidene oxazolidones (2a-b)

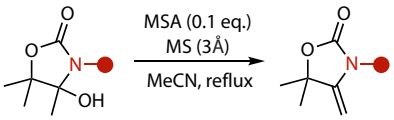

The hydroxyoxazolidone **1** (10 mmol, 1 eq.), MSA (1 mmol, 0.1 eq.) and acetonitrile (around 30 mL) were added to a round-bottom flask. A dehydration setup was installed on the flask and the mixture was refluxed for 24h. The crude was quenched with triethylamine (0.2 eq.) and cooled to room temperature. Ethyl acetate (50 mL) was added and extracted with water (3 x 50 mL). The organic phase was dried over $MgSO_4$, filtered, and dried under vacuum to yield pure **2**.

Synthesis of 5,5-dimethyl-4-methylene-3-propyloxazolidin-2-one (2a)

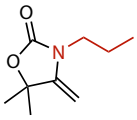

The pure product was isolated as a yellowish liquid (1.40 g, isolated yield 83 %); **^{1}H NMR** (400 MHz, DMSO-d_6) δ 4.21 (d, J = 2.6 Hz, 1H), 4.17 (d, J = 2.6 Hz, 1H), 3.36 (t, J = 7.1 Hz, 2H), 1.54 (sextuplet, J = 7.1 Hz, 2H), 0.85 (t, J = 7.5 Hz, 3 H); **^{13}C NMR** (100 MHz, DMSO-d_6) δ 155.3, 150.7, 82.1, 80.1, 42.5, 28.0, 19.7, 11.3.

Synthesis of 3-benzyl-5,5-dimethyl-4-methyleneoxazolidin-2-one (2b)

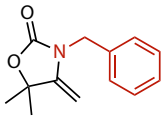

The pure product was isolated as a grayish oil (1.67 g, isolated yield 77 %); **^{1}H NMR** (400 MHz, DMSO-d_6) δ 7.31 (m, 5H), 4.62 (s, 2H), 4.16 (d, J = 2.7 Hz, 1H), 4.12 (d, J = 2.7 Hz, 1H), 1.48 (s, 6H); **^{13}C NMR** (100 MHz, DMSO-d_6) δ 155.5, 150.2, 136.3, 129.1, 127.9, 127.3, 82.6, 81.3, 44.5, 28.0.

3. Kinetic studies

A. Kinetics of reaction

Model reactions between alkylidene oxazolidones **2a-b** and thiols (benzyl mercaptan, octanethiol and thiophenol) were carried out under various conditions. The two components were mixed in equimolar ratio in a solvent with MSA and aliquots of the reaction mixture were sampled over time. The reactions were monitored by ^{1}H-NMR spectroscopy to determine the conversion in **2** at different time points. Representative NMR spectra for the different model reactions are shown in Figures S2-5 together with the resonances used for quantification.
Solvents used for the model reactions were dried over molecular sieves before use.

General procedure

2 (4 mmol, 1 eq.) and benzyl mercaptan (4 mmol, 1 eq.) were added to a reaction tube and the mixture was dissolved in 1 mL of solvent. The reaction was started by addition of MSA (0.01 eq.) and the mixture was stirred under nitrogen atmosphere.
To prepare the NMR sample, an aliquot was taken out of the reaction medium (100 µL) and was quenched with triethylamine. DMSO-d_6 (700 µL) was added and the tube was stored at -20 °C prior NMR analysis.

Model reaction of **2a** and benzyl mercaptan

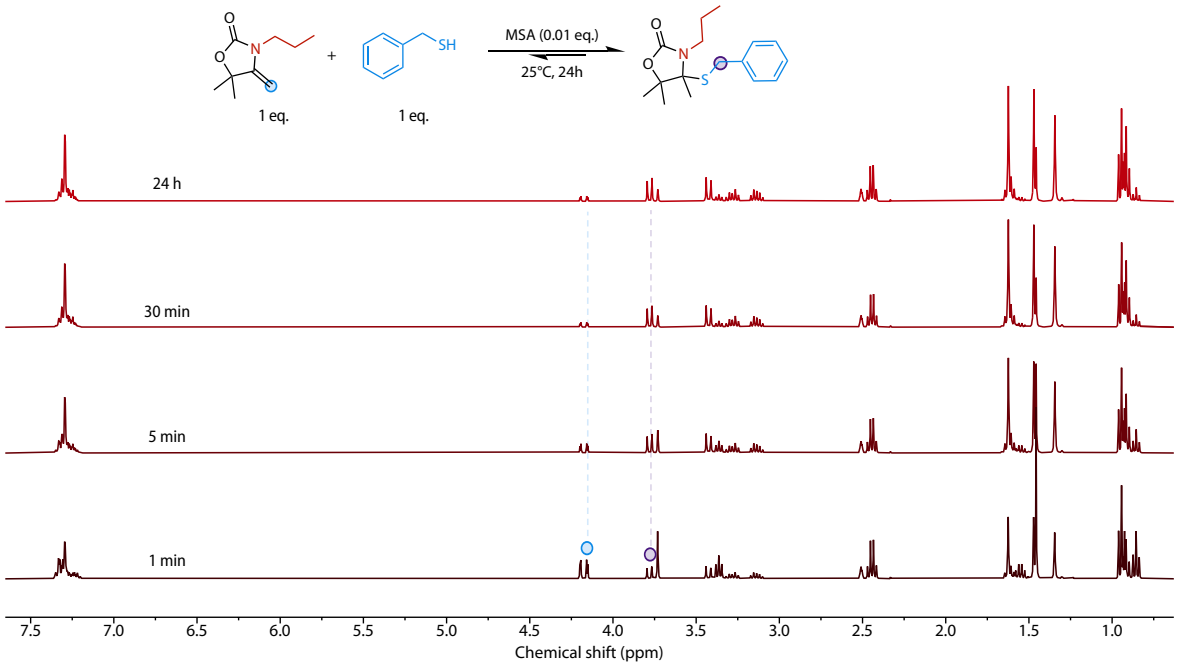

Figure S2 – Stacked ^{1}H-NMR spectra (400 MHz, DMSO-d_6) for the reaction of **2a** with benzyl mercaptan at 25°C along time.

For the reaction between **2a** and benzyl mercaptan, the resonance at 4.15 ppm (1H) was selected to follow **2a** and the resonance at 3.78 ppm (1H) to follow the product **3a**.
The following equation was used to determine the conversion:

$$Conv.(\%) = \left(\frac{I(3.78)}{I(4.15) + I(3.78)}\right) \times 100$$

Where *I* is the integral value of the selected peak.

Model reaction of **2a** and thiophenol

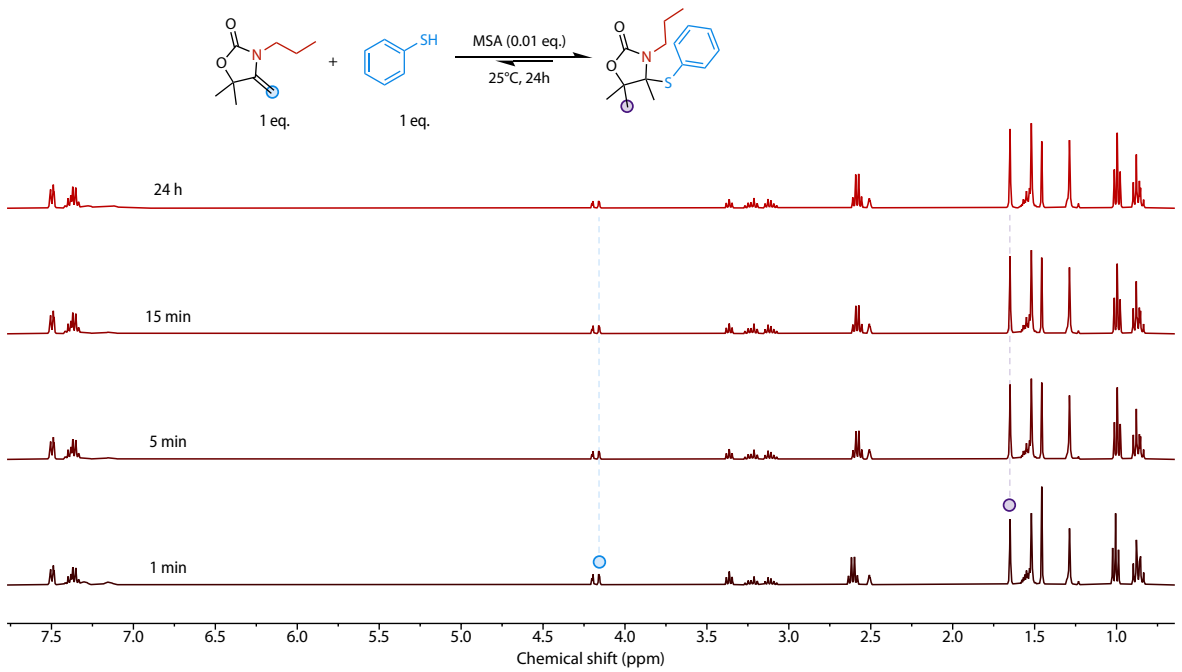

Figure S3 – Stacked ^{1}H-NMR spectra (400 MHz, DMSO-d_6) for the reaction of **2a** with thiophenol at 25°C along time.

For the reaction between **2a** and thiophenol, the resonance at 4.15 ppm (1H) was selected to follow **2a** and the resonance at 1.65 ppm (3H) to follow the product **3b**.
The following equation was used to determine the conversion:

$$Conv.(\%) = \left(\frac{\frac{I(1.65)}{3}}{I(4.15) + \frac{I(1.65)}{3}}\right) \times 100$$

Where *I* is the integral value of the selected peak.

Model reaction of **2a** and octanethiol

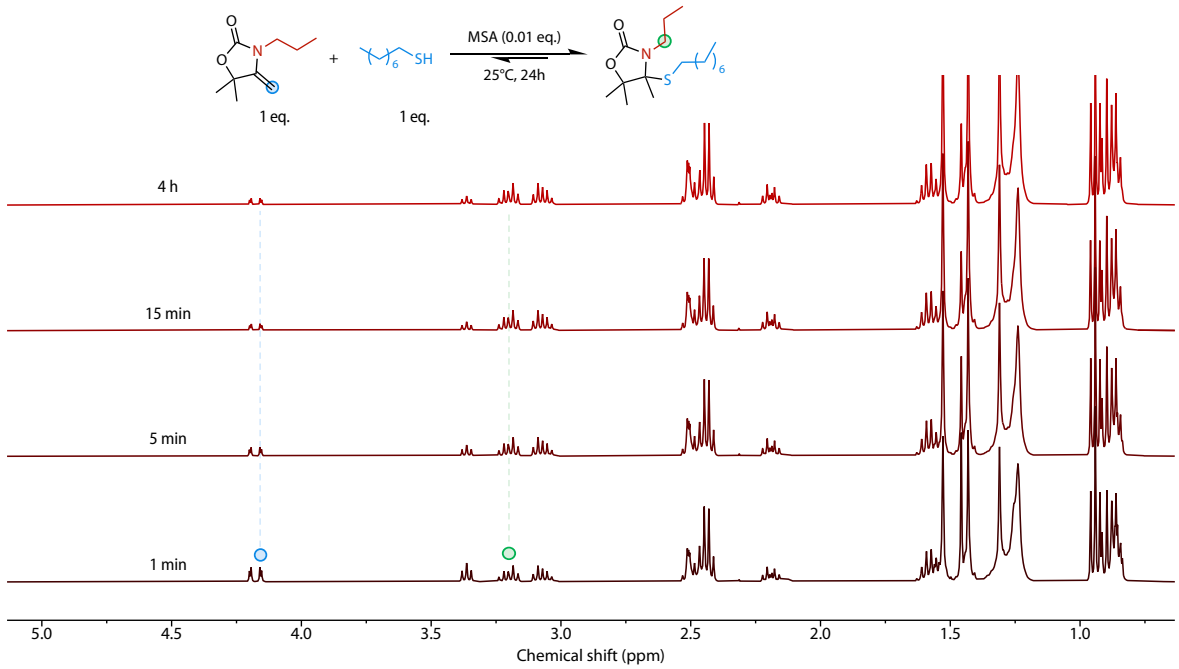

Figure S4 – Stacked ^{1}H-NMR spectra (400 MHz, DMSO-d_6) for the reaction of **2a** with octanethiol at 25°C along time.

For the reaction between **2a** and octanethiol, the resonance at 4.15 ppm (1H) was selected to follow **2a** and the resonance at 3.18 ppm (1H) to follow the product **3c**.
The following equation was used to determine the conversion:

$$Conv.\,(\%) = \left(\frac{I(3.18)}{I(4.15) + I(3.18)}\right) \times 100$$

Where I is the integral value of the selected peak.

Model reaction of **2b** and octanethiol

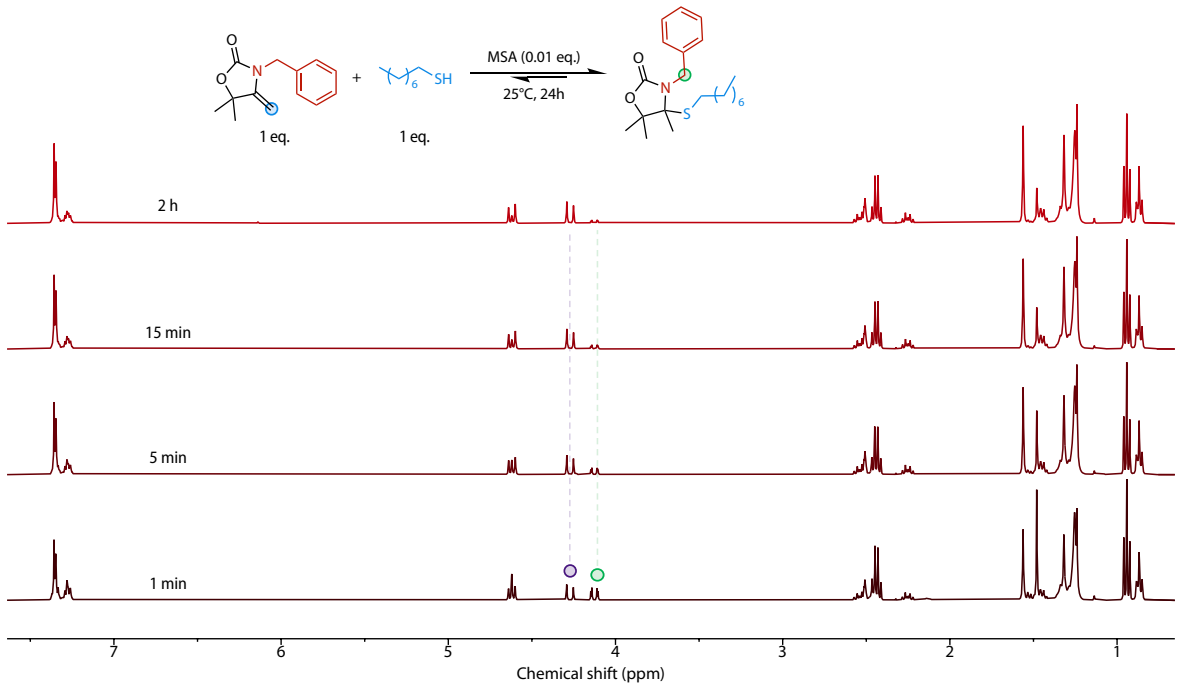

Figure S5 – Stacked ^{1}H-NMR spectra (400 MHz, DMSO-d_6) for the reaction of **2b** with octanethiol at 25°C along time.

For the reaction between **2a** and octanethiol, the resonance at 4.10 ppm (1H) was selected to follow **2b** and the resonance at 4.27 ppm (1H) to follow the product **3d**.
The following equation was used to determine the conversion:

$$Conv.\,(\%) = \left(\frac{I(4.27)}{I(4.10) + I(4.27)}\right) \times 100$$

Where *I* is the integral value of the selected peak.

Kinetic studies results

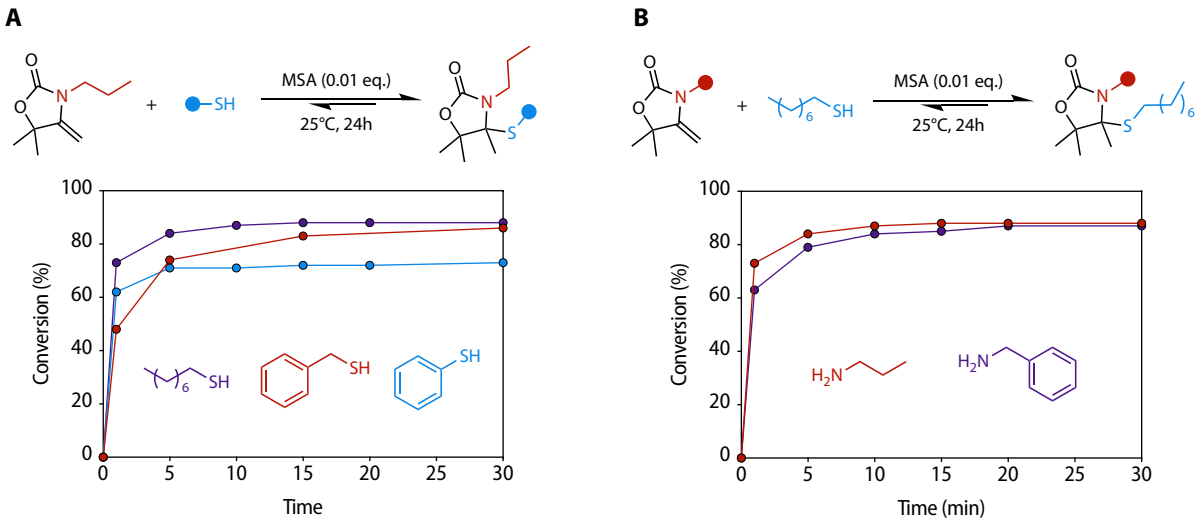

Figure S6 – Model reaction kinetic profiles for the reaction in $CHCl_3$ between (A) **2a** and different thiols and (B) **2a** or **2b** with octanethiol.

4. Synthetic Procedures: *N,S*-acetal oxazolidone compounds

General procedure for the synthesis of N,S-oxazolidones (3a-d)

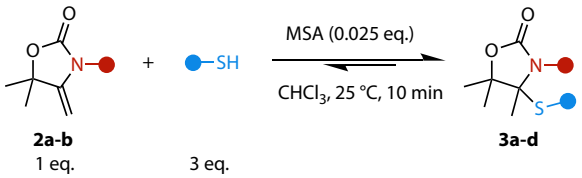

The oxazolidone **2** (3 mmol, 1 eq.), the thiol (9 mmol, 3 eq.) and 0.75 mL of $CHCl_3$ were added to a vial. MSA (7.2 mg, 0.075 mmol, 0.025 eq.) was added to the solution and the mixture was stirred for 10 minutes at 25 °C under air. The reaction was quenched by the addition of triethylamine (23 mg, 0.225 mmol, 0.075 eq.) and the crude medium was diluted with $CHCl_3$ (75 mL). The organic phase was then extracted 3 times with 75 mL NaOH aq. solution (1M) to remove the excess thiol and one time with 75 mL water. The organic phase was dried over $MgSO_4$ and dried under vacuum. The residue was purified by silica gel chromatography with diethylether / hexane (25/75).

4-(benzylthio)-4,5,5-trimethyl-3-propyloxazolidin-2-one (3a)

White solid (677 mg, isolated yield 77 %); mp = 43 °C; **^{1}H NMR** (400 MHz, DMSO-d_6) δ 7.35-7.22 (m, 5H), 3.78 (d, J = 11 Hz, 1H), 3.42 (d, J = 11 Hz, 1H), 3.32-3.22 (m, 1H), 3.18-3.08 (m, 1H), 1.62 (s, 3H), 1.61 (sextuplet, J = 7.4 Hz, 2H), 1.48 (s, 3H), 1.34 (s, 3H), 0.91 (t, J = 7.4 Hz, 3H); **^{13}C NMR** (100 MHz, DMSO-d_6) δ 156.8, 136.9, 129.4, 129.0, 127.7, 85.6, 79.1, 42.5, 34.1, 25.3, 23.6, 22.6, 20.8, 11.8. **HRMS (ESI)**: Calculated for $C_{16}H_{23}NO_2S$ $[M+Na]^+$: 316.1347. Found: 316.1347.

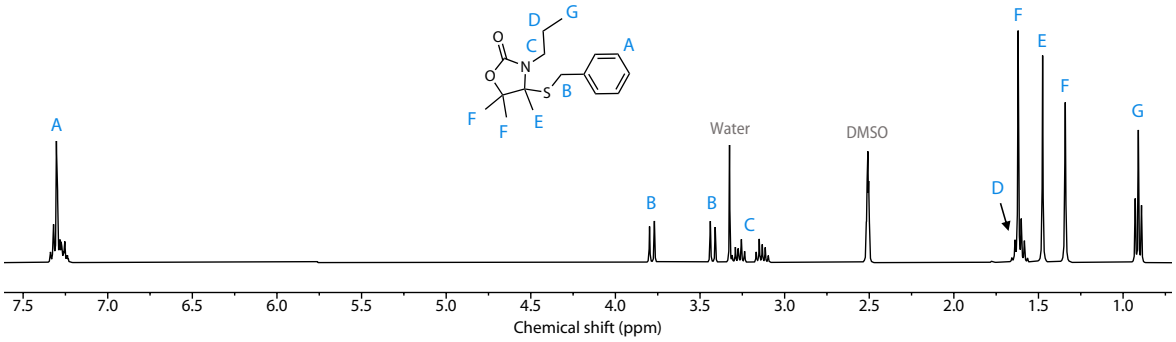

Figure S7 – ^{1}H-NMR spectrum (400 MHz, DMSO-d_6) of **3a**.

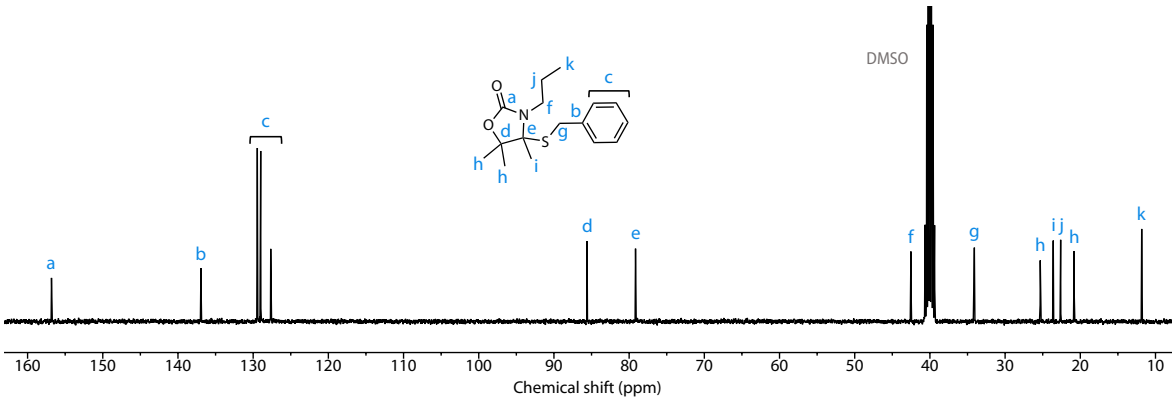

Figure S8 – ^{13}C-NMR spectrum (100 MHz, DMSO-d_6) of **3a**.

4,5,5-trimethyl-4-(phenylthio)-3-propyloxazolidin-2-one (3b)

White solid (670 mg, isolated yield 80 %); mp = 60 °C; **^{1}H NMR** (400 MHz, DMSO-d_6) δ 7.52-7.47 (m, 2H), 7.43-7.32 (m, 3H), 3.27-3.18 (m, 1H), 3.16-3.07 (m, 1H), 1.65 (s, 3H), 1.54 (sextuplet, J = 7.6 Hz, 2H), 1.52 (s, 3H), 1.29 (s, 3H), 0.88 (t, J = 7.4 Hz, 3H); **^{13}C NMR** (100 MHz, DMSO-d_6) δ 156.2, 137.0, 131.0, 129.8, 129.5, 86.1, 82.6, 43.1, 25.6, 23.3, 22.9, 21.1, 11.8. **HRMS (ESI)**: Calculated for $C_{15}H_{21}NO_2S$ $[M+K]^+$: 318.0930. Found: 318.0927.

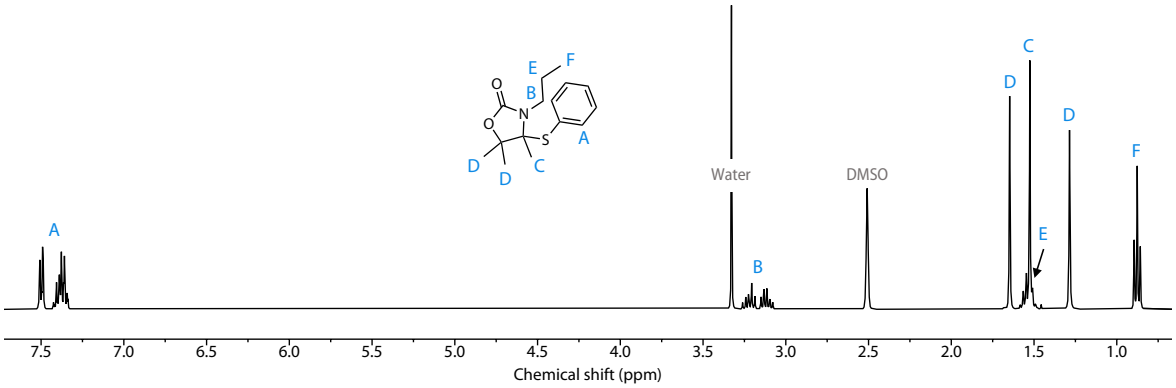

Figure S9 – ^{1}H-NMR spectrum (400 MHz, DMSO-d_6) of **3b**.

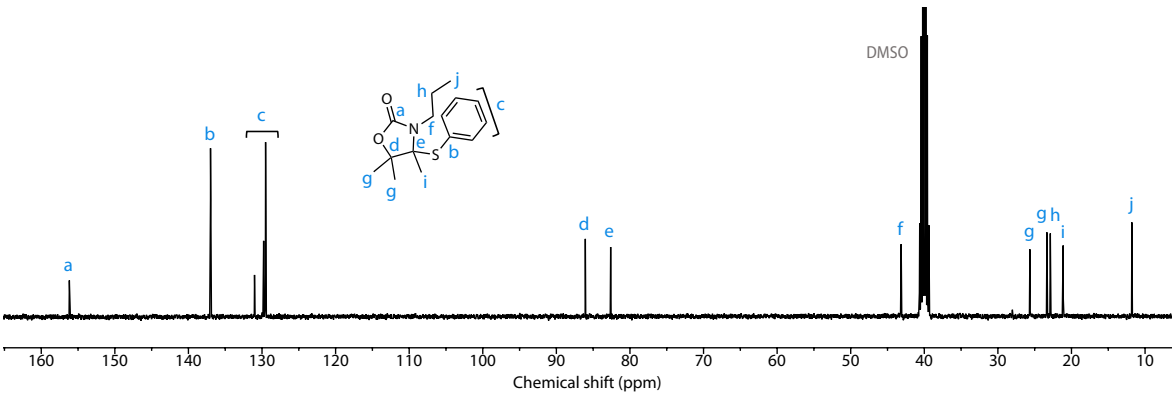

Figure S10 – ^{13}C-NMR spectrum (100 MHz, DMSO-d_6) of **3b**.

4,5,5-trimethyl-4-(octylthio)-3-propyloxazolidin-2-one (3c)

Colorless oil (813 mg, isolated yield 86 %); **^{1}H NMR** (400 MHz, DMSO-d_6) δ 3.24-3.13 (m, 1H), 3.11-3.00 (m, 1H), 2.54-2.45 (m, 1H), 2.23-2.14 (m, 1H), 1.58 (sextet, J = 7.4 Hz, 2H), 1.52 (s, 3H), 1.48-1.38 (m, 2H), 1.43 (s, 3H), 1.35-1.18 (m, 10H), 1.30 (s, 3H), 0.88 (t, J = 7.4 Hz, 3H), 0.85 (t, J = 7.1 Hz, 3H); **^{13}C NMR** (100 MHz, DMSO-d_6) δ 156.8, 85.5, 78.3, 42.5, 31.7, 29.2, 29.0, 28.9, 28.8, 28.6, 25.6, 23.5, 22.6, 22.5, 21.2, 14.4, 11.8. **HRMS (ESI)**: Calculated for $C_{17}H_{33}NO_2S$ $[M+Na]^+$: 338.2130. Found: 338.2125.

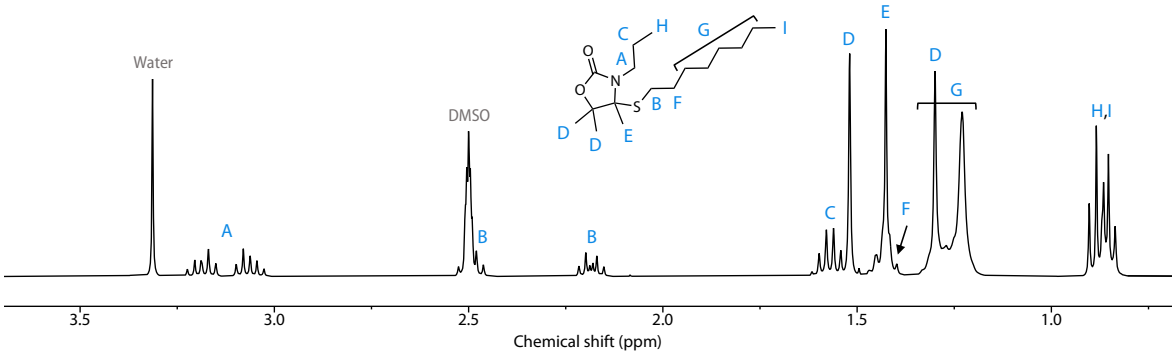

Figure S11 – ^{1}H-NMR spectrum (400 MHz, DMSO-d$_6$) of **3c**.

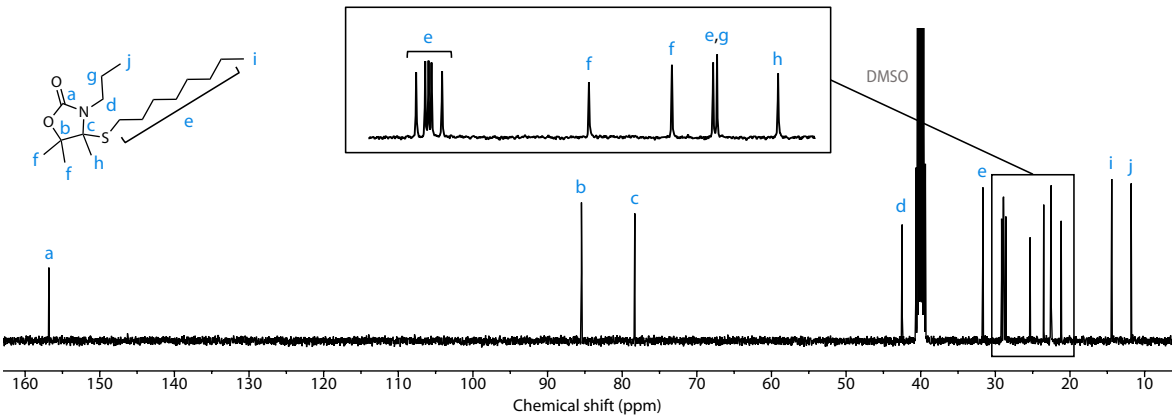

Figure S12 – ^{13}C-NMR spectrum (100 MHz, DMSO-d$_6$) of **3c**.

3-benzyl-4,5,5-trimethyl-4-(octylthio)oxazolidin-2-one (3d)

Colorless oil (969 mg, isolated yield 89 %); **^{1}H NMR** (400 MHz, DMSO-d$_6$) δ 7.39-7.32 (m, 4H), 7.32-7.24 (m, 1H), 4.60 (d, J = 15.9 Hz, 1H), 4.28 (d, J = 15.9 Hz, 1H), 2.58-2.49 (m, 1H), 2.29-2.20 (m, 1H), 1.56 (s, 3H), 1.51-1.39 (m, 2H), 1.37-1.2 (m, 10H), 1.32 (s, 3H), 1.24 (s, 3H), 0.91-0.82 (m, 3H); **^{13}C NMR** (100 MHz, DMSO-d$_6$) δ 157.2, 138.6, 129.0, 127.8, 127.7, 85.9, 78.5, 44.2, 31.7, 29.2, 29.0, 28.95, 28.90, 28.6, 25.5, 23.5, 22.5, 21.3, 14.4. **HRMS (ESI)**: Calculated for $C_{21}H_{33}NO_2S$ [M+K]$^{+}$: 402.1869. Found: 402.1867.

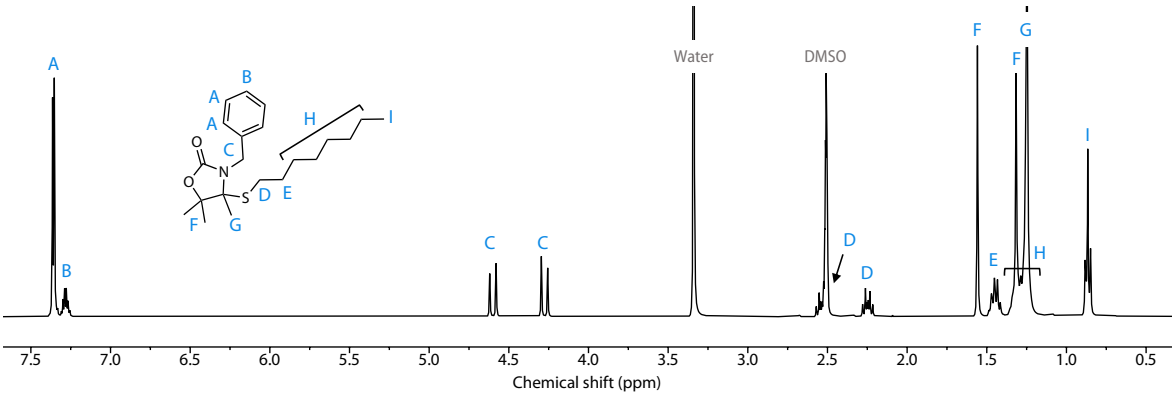

Figure S13 – ^{1}H-NMR spectrum (400 MHz, DMSO-d$_6$) of **3d**.

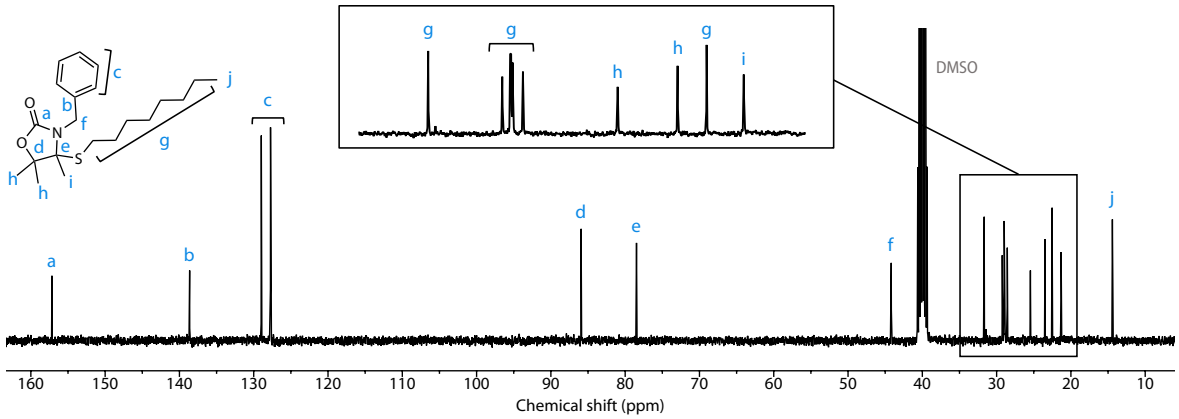

Figure S14 – ^{13}C-NMR spectrum (100 MHz, DMSO-d_6) of **3d**.

5. Computational details

Preliminary calculations of equilibrium structures were performed using a semi-empirical model (PM7)[2] to determine the most stable conformations. These semi-empirical calculations were performed using the MOPAC software[3]. The lowest energy structures obtained at the semi-empirical level were further investigated using the Density Functional Theory (DFT) method implemented in the Gaussian 16 package[4]. DFT calculations of geometries, energies and vibrational frequencies reported in this paper were carried out with the ωB97X-D functional[5] using the 6-311++G(d,p) basis set with the CPCM solvation model (chloroform). All frequencies of each structure have also been calculated to verify the presence of a single imaginary frequency for transition states and the absence of imaginary frequency for ground states. The intrinsic reaction coordinate (IRC) method has been used to verify that the obtained transition states were effectively connected to the desired minima. A wide range of possible configurations and interactions have been modelled and the more stable of them are reported in this work. To consider entropic effects, the energies mentioned in this study correspond to the Gibbs free energy.

The studied reaction pathway was discussed in the main manuscript. Intermediates on both sides of each transition states were annotated on the pathway displayed in Figure S15. Details on bond lengths along the reaction path (Figure S16, Table S1) and 3D structures of intermediates and transition states are provided here (Figure S17).

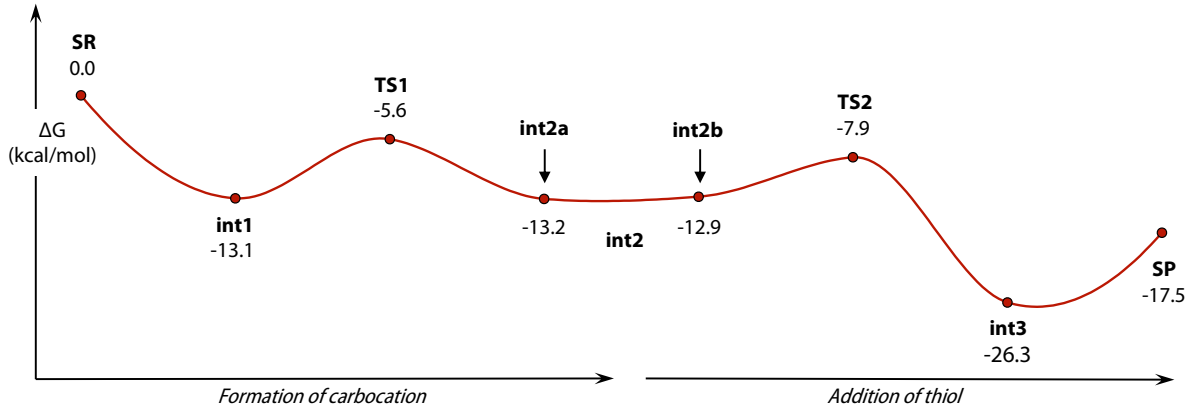

Figure S15 – Gibbs-Free Energy profile for the model reaction as studied by DFT.

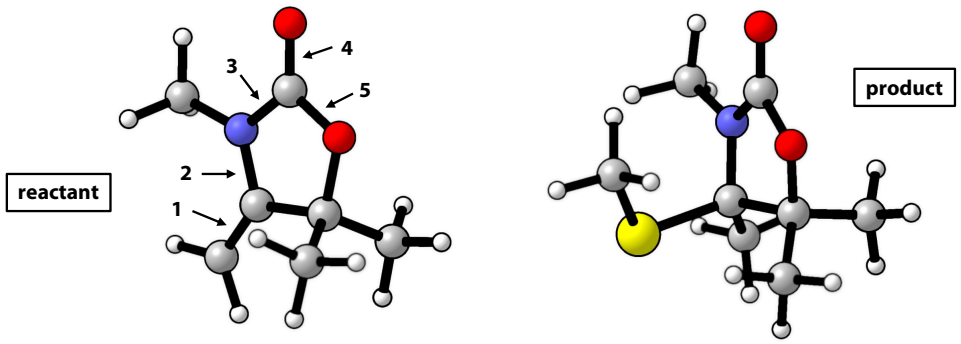

Figure S16 – 3D structures of the reactant and the product. A number was attributed to bonds whose length was followed along reaction coordinates.

Table S1 – Bond lengths for intermediates and transition states along the reaction path (expressed in Å).

	SR	int1	TS1	int2a	int2b	TS2	int3	SP
C-C (1)	1.332	1.340	1.388	1.461	1.461	1.484	1.524	1.525
C-N (2)	1.382	1.373	1.329	1.292	1.293	1.323	1.440	1.446
N-C (3)	1.382	1.379	1.413	1.452	1.450	1.423	1.366	1.363

C-O (4)	1.197	1.203	1.194	1.186	1.185	1.191	1.207	1.209
C-O (5)	1.346	1.339	1.328	1.318	1.320	1.327	1.348	1.348

From separate reactants, the partners can assemble into a stable complex whose stabilization energy is -13.1 kcal/mol. This is allowed by hydrogen bonds between the negatively charged carbon atom of the alkene and the acidic proton of MSA and between the acidic proton of the thiol and a free oxygen atom of MSA. The first interaction is already responsible for a slight bond (1) length increase of the alkene. Upon transfer of the acidic proton of MSA to the alkene through TS1, the so-formed carbocation in **int2** is stabilized by the nitrogen atom which can share electrons to build a stable pi bond. All bond lengths in the ring are strongly impacted by this step as indicated in Table S. The previous C=C alkene bond becomes a sigma C-C bond (1) with increased bond length (+0.121 Å). On the other side, the C-N bond (2) decreases with the creation of the stable pi bond. The nitrogen atom thus shares less electrons with the electron-poor carbon of the carbonyl group, resulting in a N-C(O) bond (3) length increase (+0.073 Å). Additional hydrogen bonds stabilize **int2**, rendering this intermediate as energetically stable as the reactants complex. The second step begins with **int2** where hydrogen bonds with the proton of the thiol and the proton of the oxazolidone methyl group are located on the same oxygen donor group of the MSA, whose negative charge is stabilized by these interactions. The addition of the thiol on the electrophilic carbon takes place as the proton from the thiol is transferred to the MSA. The C=N (2) pi bond is suppressed, and the bond length readily increases (+0.147 Å). The nitrogen is then able to share back more electrons with the carbonyl atom resulting in a bond (3) length decrease (-0.084 Å). The product complex **int3** is stabilized of 8.8 kcal/mol on the account of hydrogen bonding between the acidic proton of regenerated MSA and the sulfur atom of the N,S-oxazolidone.

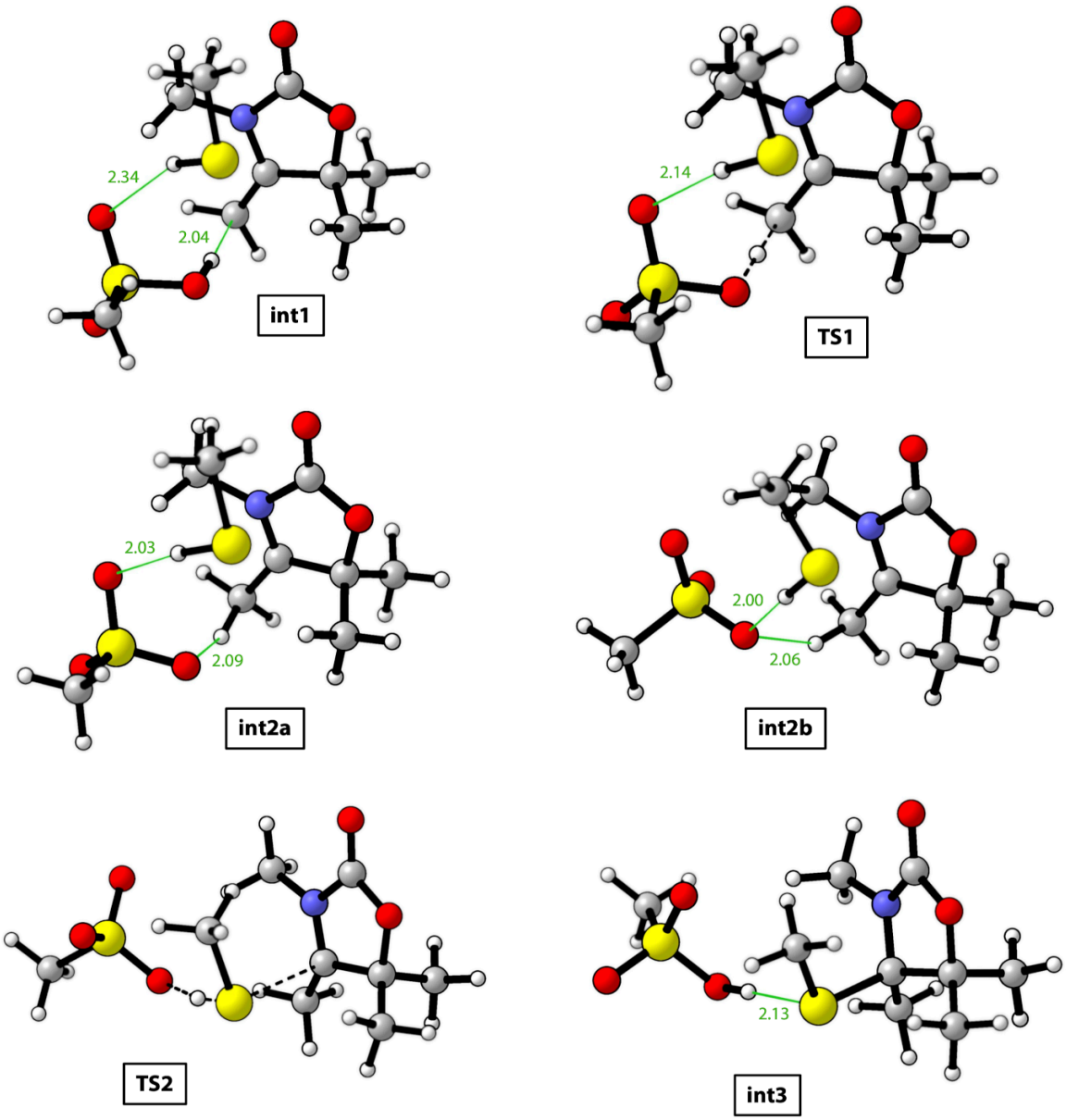

Figure S17 – 3D structures of optimized intermediates and transition states along the reaction path.

6. Model exchange reactions

The kinetics of the exchange reaction at the model molecule level was performed. **3a** was reacted with a fivefold excess of octanethiol, thus producing **3c** and benzyl mercaptan. The kinetics was performed by dissolving **3a** at a concentration of 0.25 M in $CDCl_3$. Octanethiol (5 eq.) and MSA (0.01 eq.) were added to the reaction mixture to initiate the exchange. Aliquots were taken at different times and were quenched with triethylamine prior ^{1}H-NMR analysis. Characteristic signals of **3a** and **3c** were followed to monitor the reaction (Figure S18). For **3a**, the characteristic signal of the benzyl -$\underline{CH_2}$- at 3.80 ppm (in purple) was followed. For **3c**, an overlapping signal characteristic for the N-$\underline{CH_2}$- signal of both the reactants and products was followed (in green).

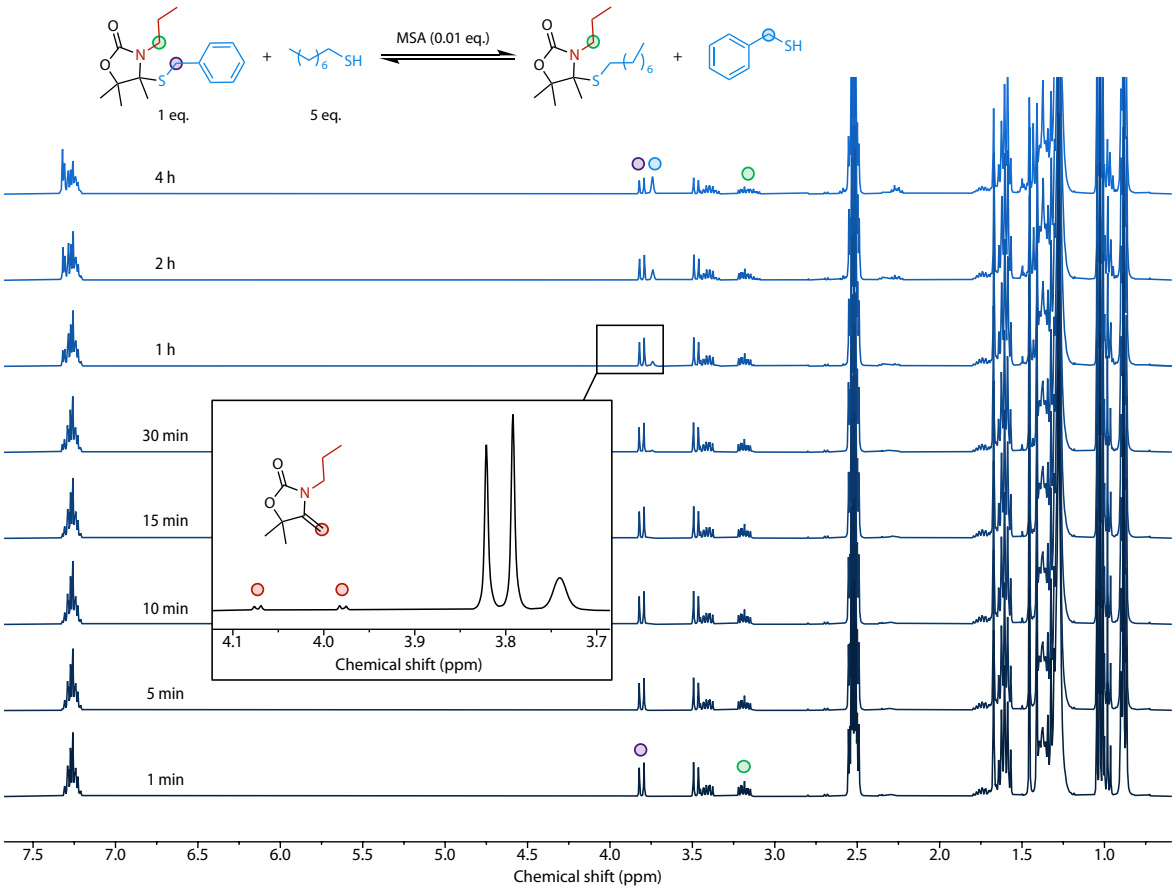

Figure S18 – Stacked ^{1}H-NMR spectra (400 MHz, $CDCl_3$) of the kinetics of the exchange reaction between **3a** and a fivefold excess of octanethiol at 25 °C.

In order to get an activation of energy for the exchange reaction, the same reaction was performed at five different temperatures (7 to 50 °C). A fit derived from the equation of the isotope exchange kinetics could be used to extract rate constants k for all the reactions(Figure S19)[6].

$$[reactant] = 1 - (x_\infty - \exp\left(\frac{-kt}{x_\infty}\right))$$

Where x_∞ is the equilibrium concentration of the product (0.8225).

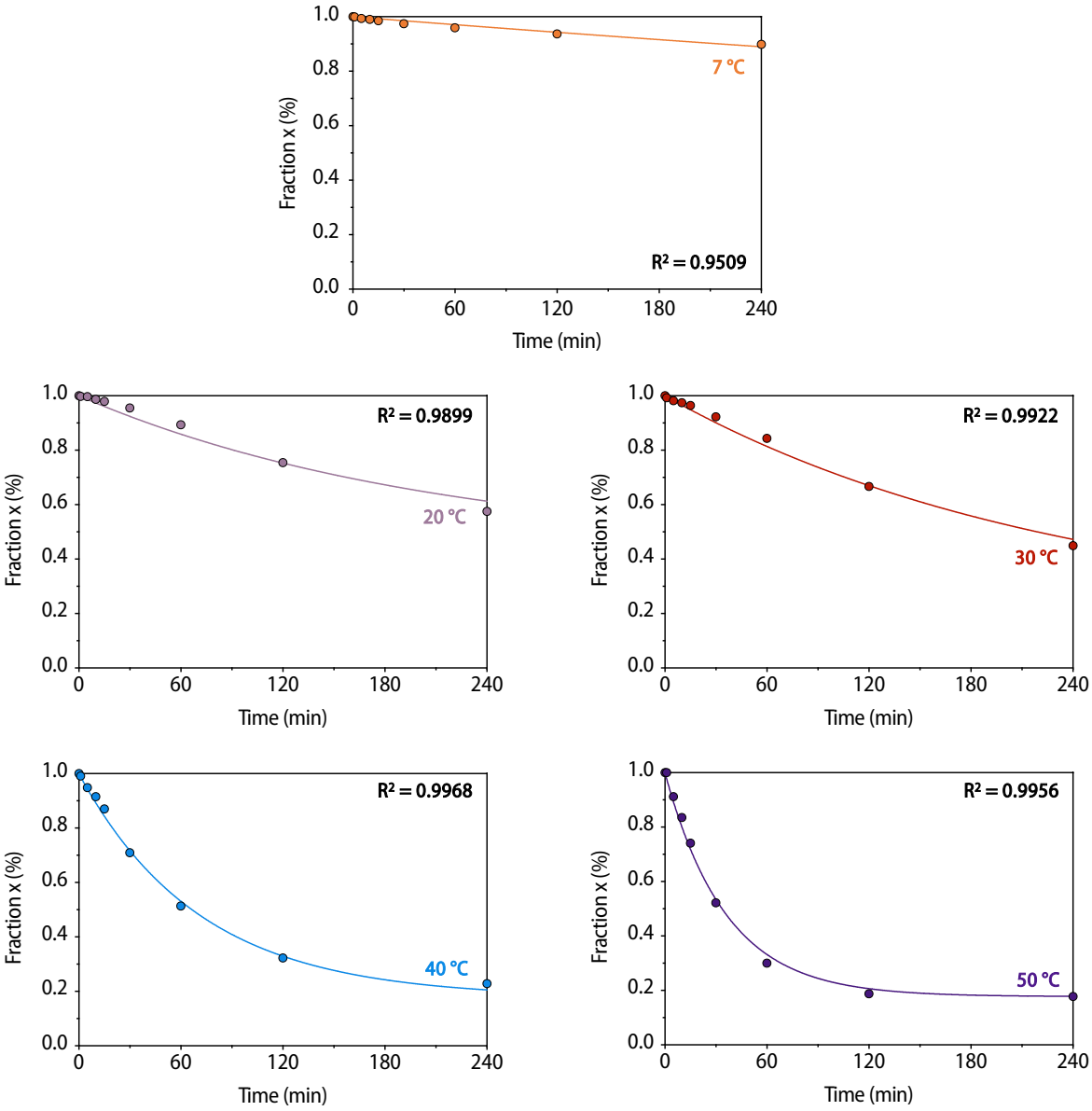

Figure S19 – Exchange reaction kinetic profiles for the reaction between **3a** and a fivefold excess of octanethiol at different temperatures. The kinetic data points (dots) were fitted to an equation to extract constant rates k (lines).

From the different rate constants at the different temperatures, an Arrhenius plot was built. From a linear regression fit, the activation of energy for the exchange reaction could be determined.

$$\ln(k) = \ln(A) - \frac{E_a}{RT}$$

Table S2 – Exchange activation energy of various dynamic bonds determined on both model compounds and polymer network matrices. Referred papers[7–14] are provided.

		Exchange activation energy (kcal/mol)		Ref.
Dynamic bond	Catalyst	Model compound	Polymer	
N,S-oxazolidone	MSA	15.5	26.4 – 38.8	
S,S-acetals	TBD	15.8 – 18.4	29.7 – 47.3	7
Vinylogous urethane	Catalyst-free	14.1	14.3	8
Vinylogous urea	Catalyst-free	12.5	10.5 – 14.3	9

Diketoenamine	Catalyst-free	6.9 – 14.8	11.7 – 14.3	10
Dioxaborolane	Catalyst-free	3.8	18.3	11
Phtalate monoster	Internal catalysis	22.9	28.7	12
Triazolinedione	$ZrAc_4$	26.0 – 27.8	25.8	13,14

7. Synthetic Procedures: alkylidene oxazolidones monomers

General procedure for the tandem synthesis of bis(alkylidene oxazolidone)s (2c-f)

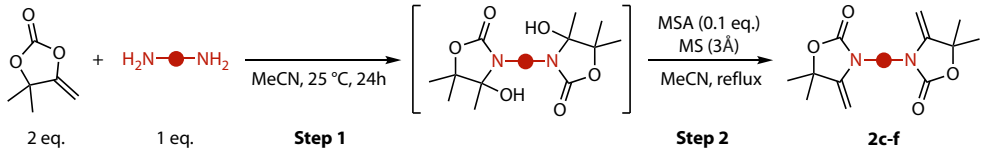

αCC (20.48 g, 0.16 mol, 2 eq.), the diamine (0.08 mol, 1 eq.) and acetonitrile (40 mL) were added to a round-bottom flask. The mixture was stirred in an ice bath for the first minutes of reaction and then at 25 °C. After 24h, MSA (0.1 eq.) and acetonitrile (80 mL) were added. The dehydration setup was installed on the flask and the mixture was refluxed for 24h. The crude was quenched with triethylamine (0.3 eq.) and cooled to room temperature. The mixture was diluted in dichloromethane (600 mL) and extracted with water (3 x 600 mL). The organic phase was dried over $MgSO_4$ and filtered. Solvent was partially removed under vacuum until around 100 mL is left. The solution was passed on a thin silica pad and 250 mL of dichloromethane is then passed on the pad. Solvent was then entirely removed under vacuum. When the monomer was solid, it was recrystallized in a suitable solvent system, filtered on Büchner, and washed with hexane to yield the pure product.
Deviations from this procedure are given for each product.

3,3'-(1,3-phenylenebis(methylene))bis(5,5-dimethyl-4-methyleneoxazolidin-2-one) (2c)

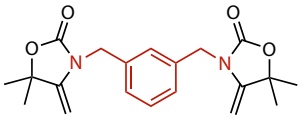

Recrystallized in Ethyl acetate 25 / Hexane 75 to yield white crystals (22.9 g, isolated yield 80%); mp = 107 °C; **^{1}H NMR** (400 MHz, DMSO-d_6) δ 7.34 (t, J = 7.5 Hz, 1H), 7.21 (d, J = 7.5 Hz, 2H), 7.08 (s, 1H), 4.60 (s, 4H), 4.13 (d, J = 2.7 Hz, 2H), 4.06 (d, J = 2.7 Hz, 2H), 1.46 (s, 6H); **^{13}C NMR** (100 MHz, DMSO-d_6) δ 155.4, 150.1, 136.8, 129.3, 126.7, 124.8, 82.6, 81.2, 44.36, 27.94. **HRMS (ESI)**: Calculated for $C_{20}H_{25}N_2O_4$ $[M+H]^+$: 357.1814. Found: 357.1820.

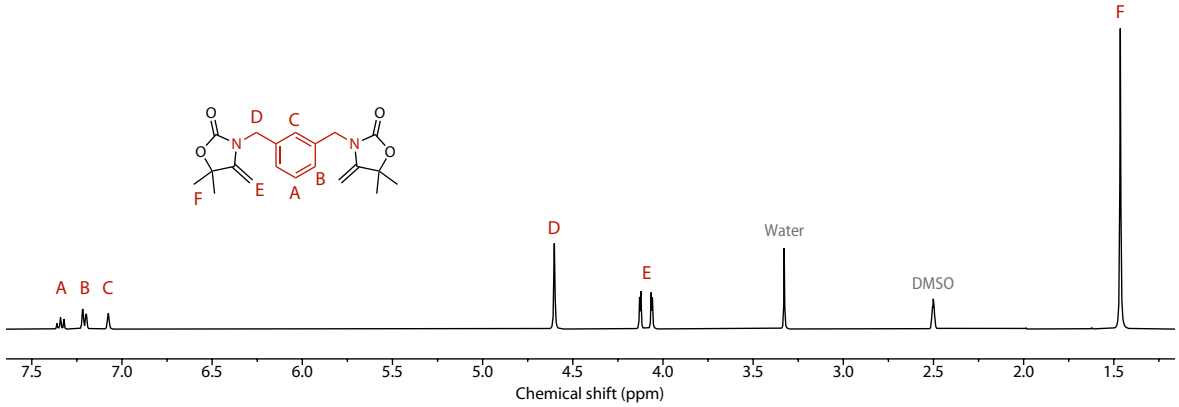

Figure S20 – ^{1}H-NMR spectrum (400 MHz, DMSO-d_6) of **2c**.

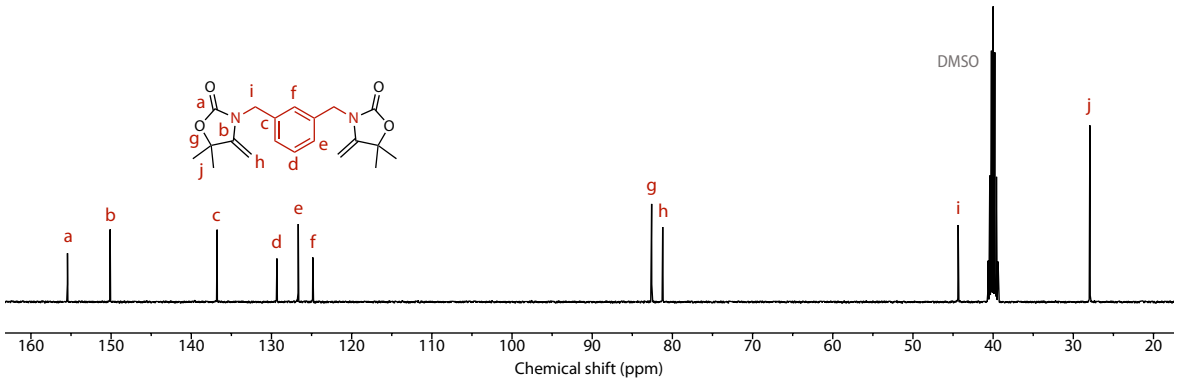

Figure S21 – ^{13}C-NMR spectrum (100 MHz, DMSO-d$_6$) of **2c**.

3,3'-((ethane-1,2-diylbis(oxy))bis(ethane-2,1-diyl))bis(5,5-dimethyl-4-methyleneoxazolidin-2-one) (2d)

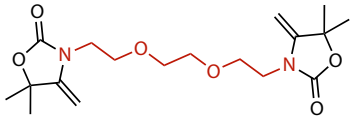

For the first step, DBU (0.05 eq.) was added to the reaction mixture. For the second step, 0.15 eq. of MSA was used rather than 0.1 eq. Recrystallized in Chloroform 10 / Hexane 90 to yield white crystals (22.8 g, isolated yield 77%); mp = 101 °C; **^{1}H NMR** (400 MHz, DMSO-d$_6$) δ 4.26 (d, J = 2.7 Hz, 2H), 4.18 (d, J = 2.7 Hz, 2H), 3.55 (s, 8H), 3.49 (s, 4H), 1.45 (s, 6H); **^{13}C NMR** (100 MHz, DMSO-d$_6$) δ 155.2, 150.5, 82.2, 80.5, 70.1, 66.2, 40.9, 27.94. **HRMS (ESI)**: Calculated for $C_{18}H_{29}N_2O_6$ $[M+H]^+$: 369.2026. Found: 369.2023.

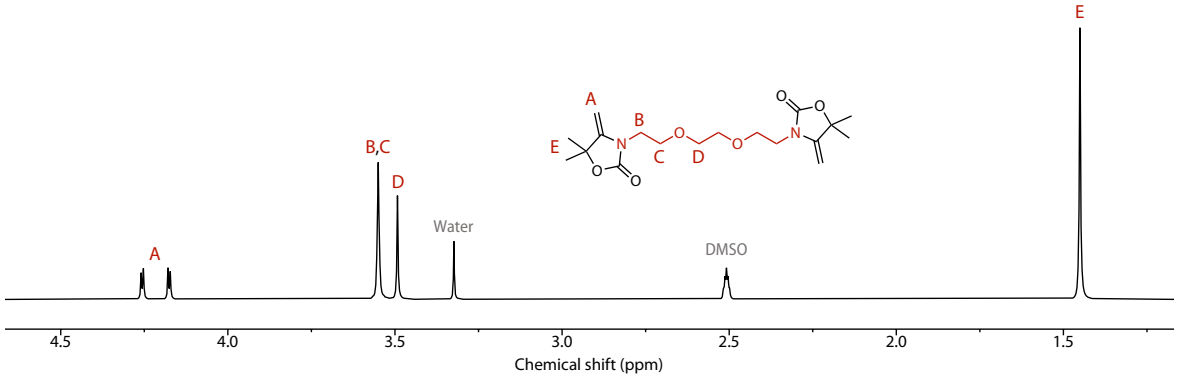

Figure S22 – ^{1}H-NMR spectrum (400 MHz, DMSO-d$_6$) of **2d**.

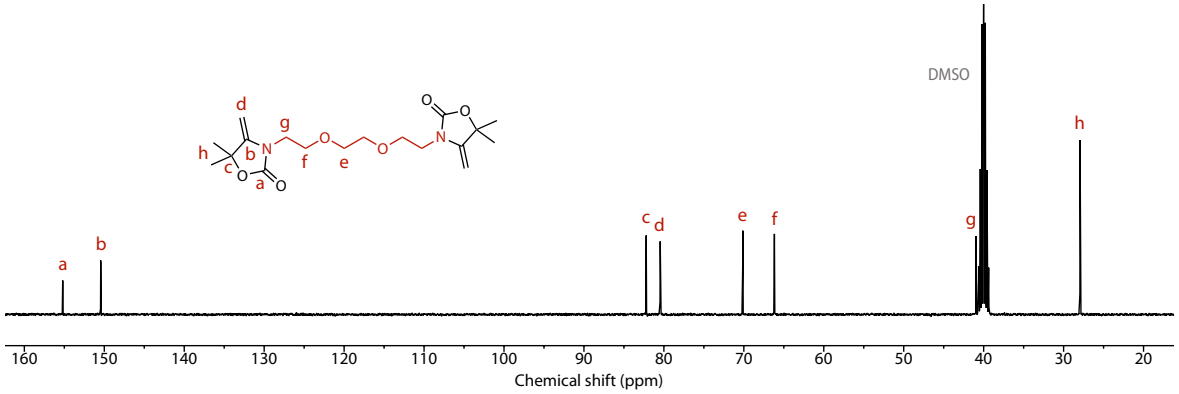

Figure S23 – ^{13}C-NMR spectrum (100 MHz, DMSO-d$_6$) of **2d**.

3,3'-(hexane-1,6-diyl)bis(5,5-dimethyl-4-methyleneoxazolidin-2-one) (2e)

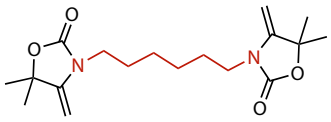

For the first step, DBU (0.05 eq.) was added to the reaction mixture. For the second step, 0.15 eq. of MSA was used rather than 0.1 eq. Recrystallized in Diethyl ether 40 / Hexane 60 to yield white crystals (22.65 g, isolated yield 84%); mp = 66 °C; **^{1}H NMR** (400 MHz, DMSO-d_6) δ 4.19 (d, J = 2.7 Hz, 2H), 4.16 (d, J = 2.7 Hz, 2H), 3.37 (t, J = 7.1 Hz, 4H), 1.55-1.46 (m, 4H), 1.44 (s, 12H), 1.33-1.21 (m, 4H); **^{13}C NMR** (100 MHz, DMSO-d_6) δ 155.2, 150.6, 82.1, 80.1, 40.9, 28.0, 26.2, 26.0. **HRMS (ESI)**: Calculated for $C_{18}H_{29}N_2O_4$ $[M+H]^+$: 337.2127. Found: 337.2122.

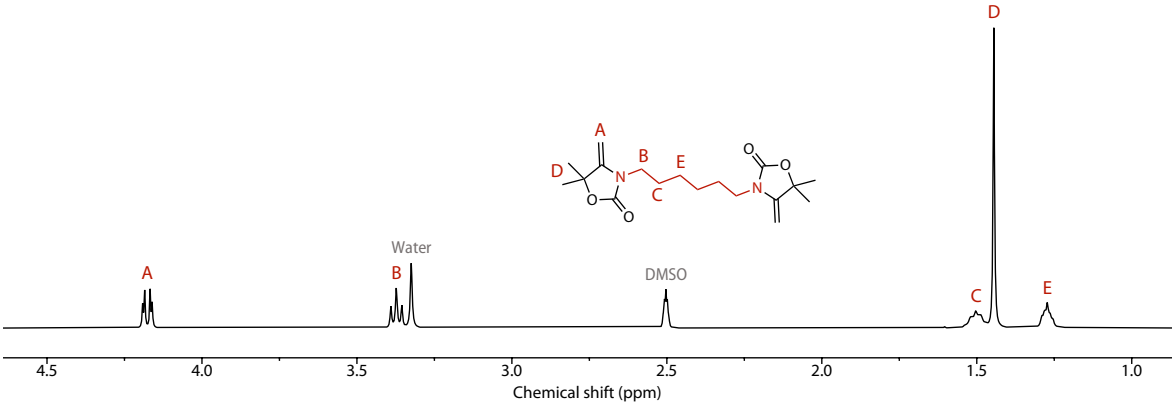

Figure S24 – ^{1}H-NMR spectrum (400 MHz, DMSO-d_6) of **2e**.

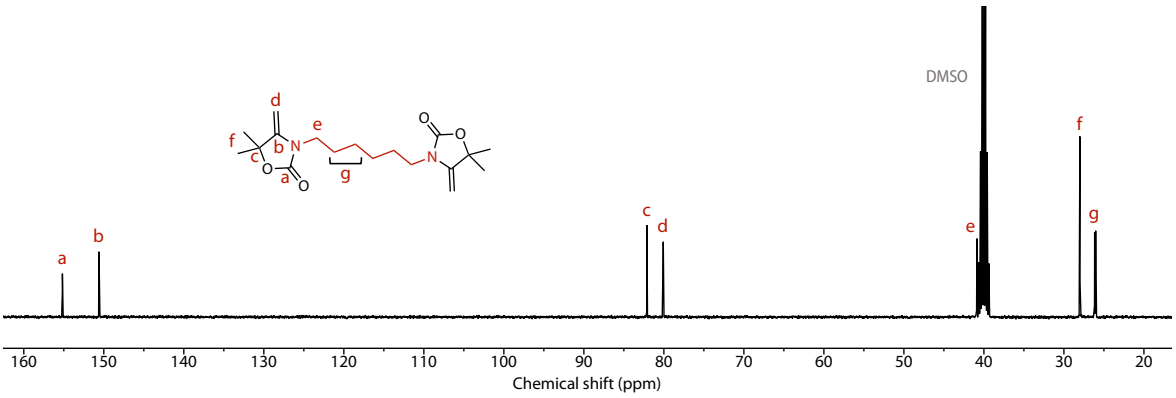

Figure S25 – ^{13}C-NMR spectrum (100 MHz, DMSO-d_6) of **2e**.

Bis(alkylidene oxazolidone) from Priamine 1075 PRI (2f)

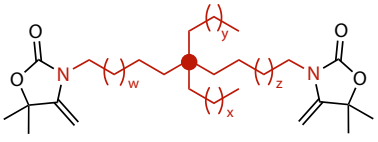

Instead of acetonitrile, toluene was used for both steps. For the first step, DBU (0.05 eq.) was added to the reaction mixture. For the second step, 0.15 eq. of MSA was used rather than 0.1 eq. Isolated as pale-yellow viscous liquid (51.23 g, isolated yield 83%); **^{1}H NMR** (400 MHz, $CDCl_3$) δ 4.07 (d, J = 2.9 Hz, 2H), 3.98 (d, J = 2.9 Hz, 2H), 3.43 (t, J = 7.4 Hz, 4H) 1.66-1.54 (m, 4H), 1.49 (s, 12H), 1.45-0.99 (m, 49H), 0.97-0.71 (m, 9H); **^{13}C NMR** (100 MHz, $CDCl_3$) δ 155.6, 151.1, 81.9, 79.0, 41.5, 31.9, 29.7, 29.6, 29.5, 29.4, 29.3, 28.0, 26.7, 26.3, 22.7, 14.1.

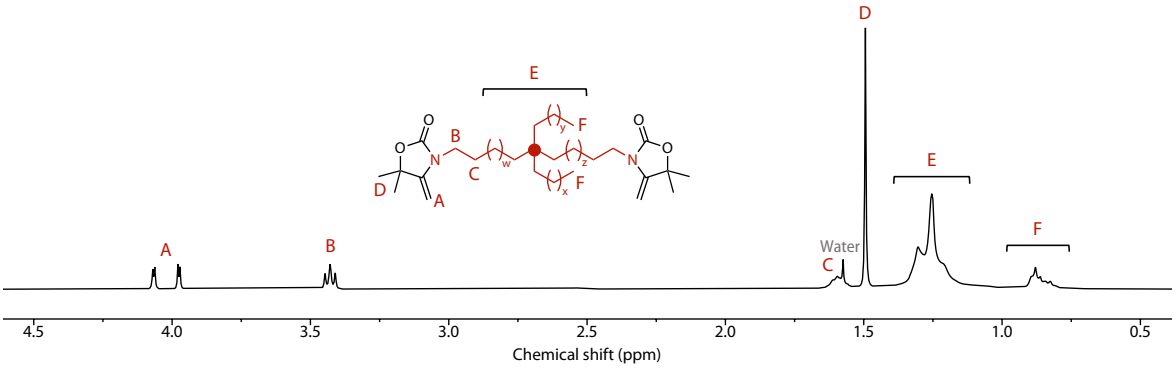

Figure S26 – ^{1}H-NMR spectrum (400 MHz, $CDCl_3$) of **2f**.

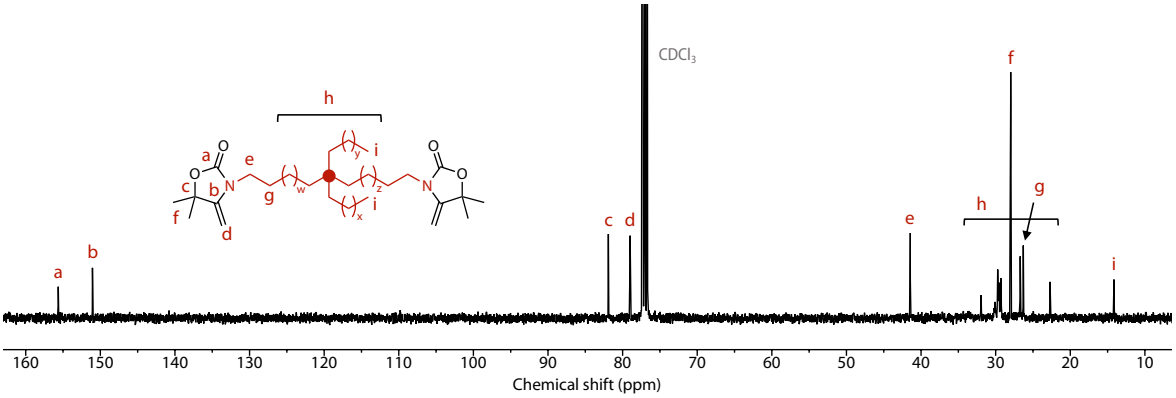

Figure S27 – ^{13}C-NMR spectrum (100 MHz, $CDCl_3$) of **2f**.

8. Polymer synthesis

In a baker containing 20 mL of $CHCl_3$ were added the monomer **2c-f** or a mix of monomers (20 mmol, 1 eq.) and PETMP (10 mmol, 0.5 eq.). Once the solution was homogeneous, MSA (0.01 eq.) was added and the mixture was stirred at room temperature. After 10 to 60 minutes, a gel was formed. The gel was easily recovered and dried under vacuum at 70 °C overnight. The pure polymer was then slowly cooled down to room temperature.

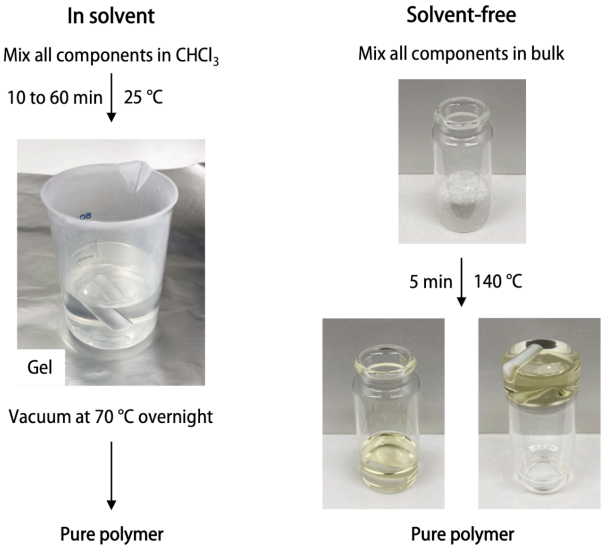

Figure S28 – Possible polymerization methods (for **P-HMDA** here): in solvent (left) and in bulk (right).

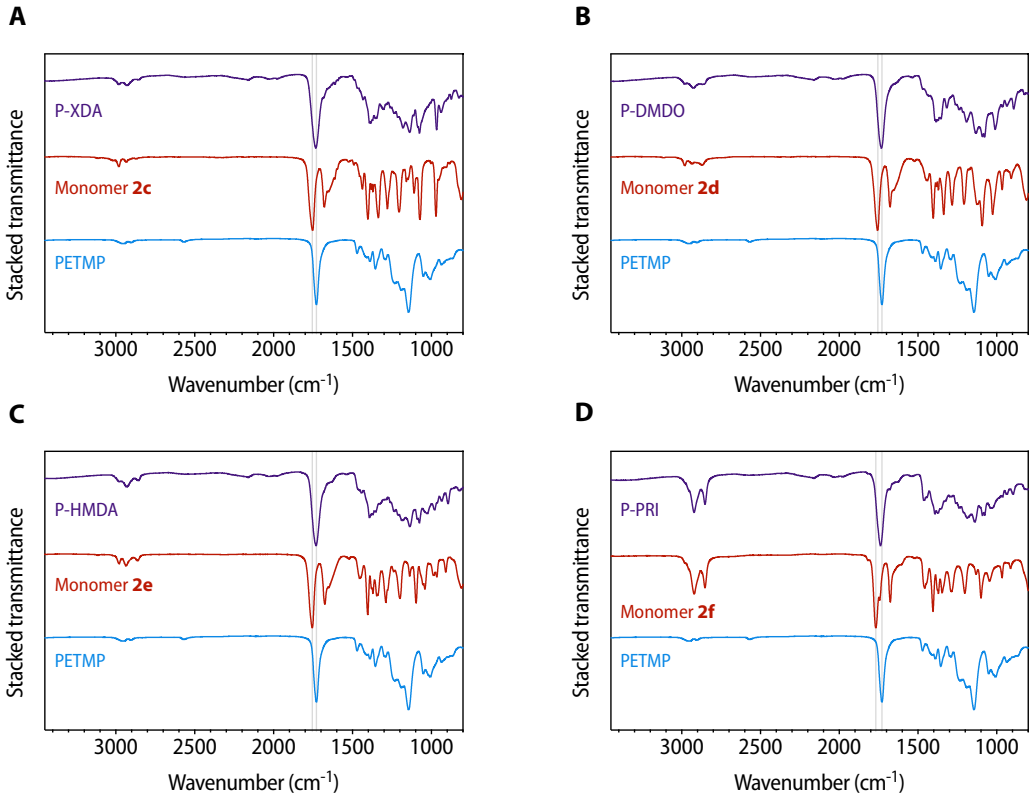

Figure S29 – ATR-IR spectra of (A) P-XDA, (B) P-DMDO, (C) P-HMDA, and (D) P-PRI and their respective monomers.

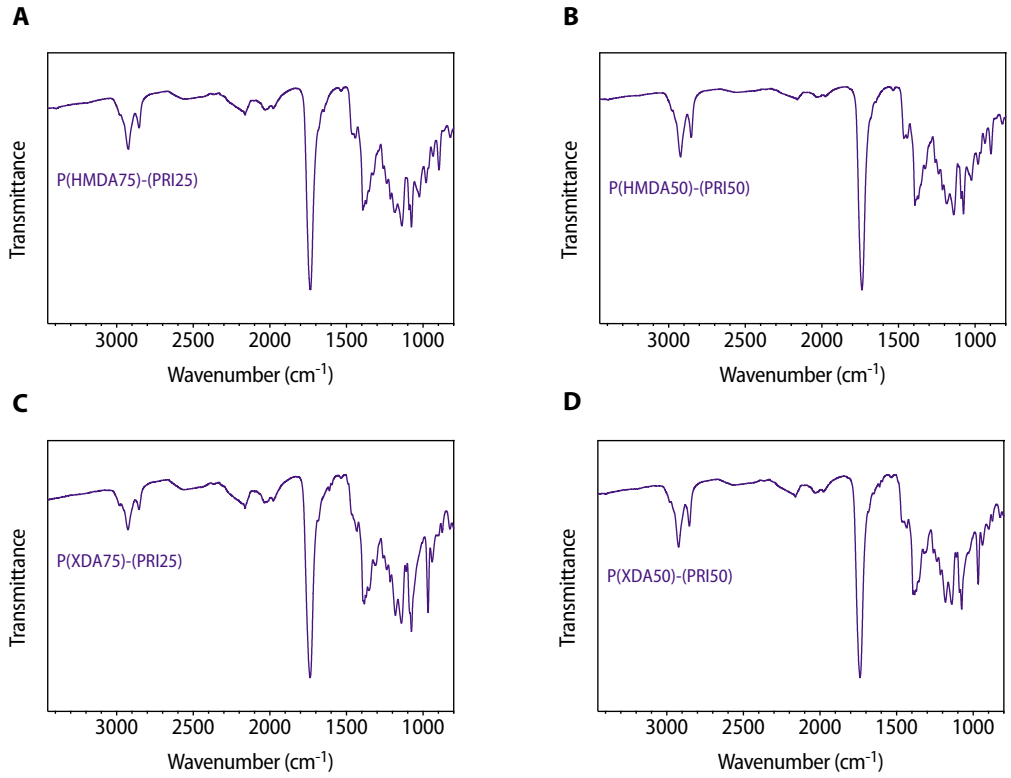

Figure S30 – ATR-IR spectra of (A) P(HMDA75)-(PRI25), (B) P(HMDA50)-(PRI50), (C) P(XDA75)-(PRI25), and (D) P(XDA50)-(PRI50).

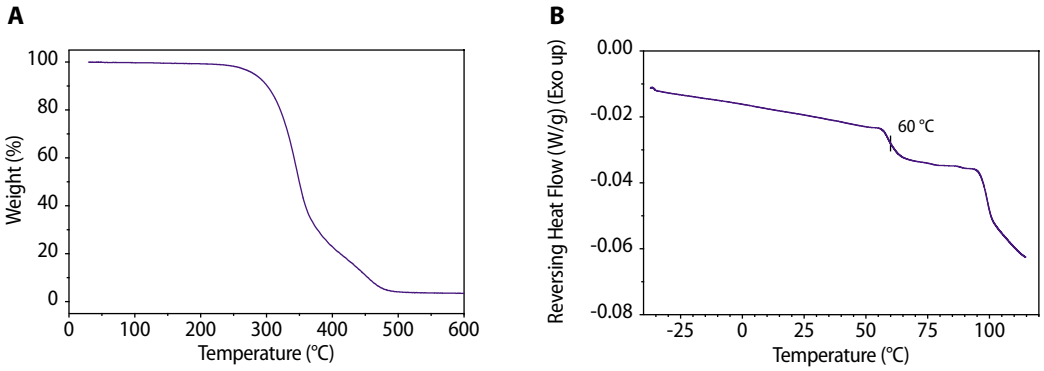

Figure S31 – (A) TGA and (B) mDSC curves for **P-XDA**.

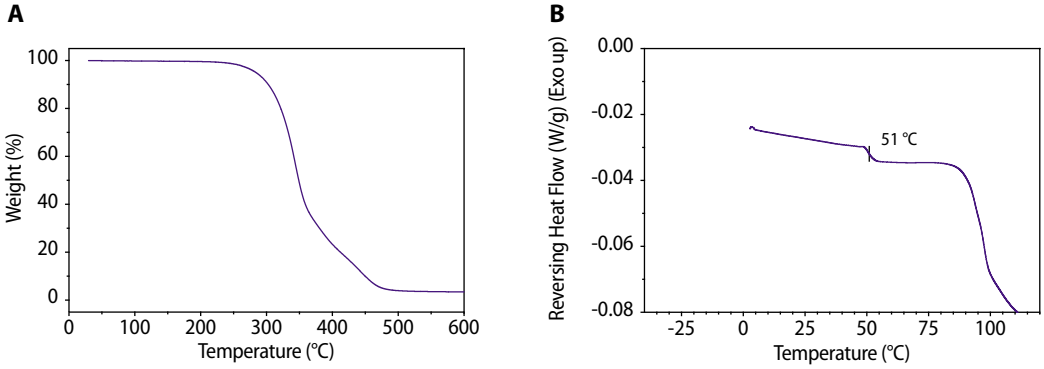

Figure S32 – (A) TGA and (B) mDSC curves for **P-DMDO**.

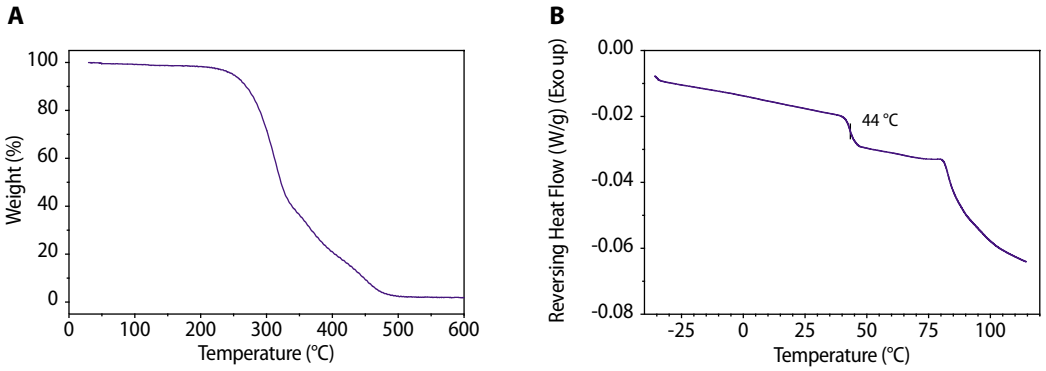

Figure S33 – (A) TGA and (B) mDSC curves for **P-HMDA**.

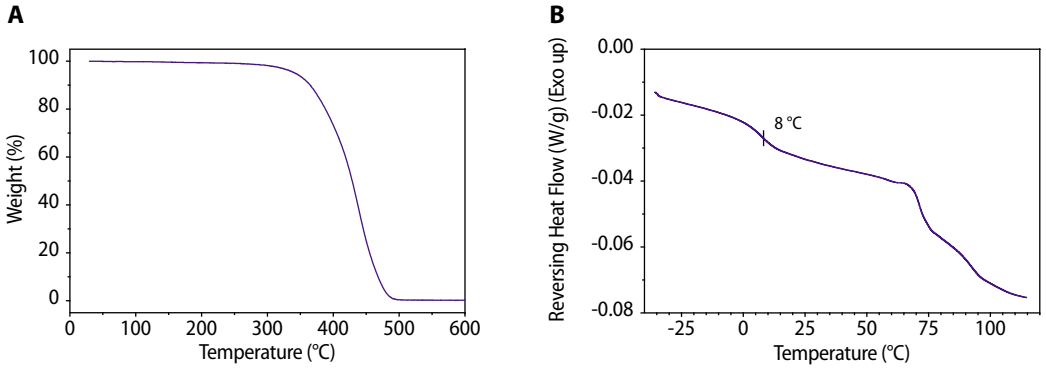

Figure S34 – (A) TGA and (B) mDSC curves for **P-PRI**.

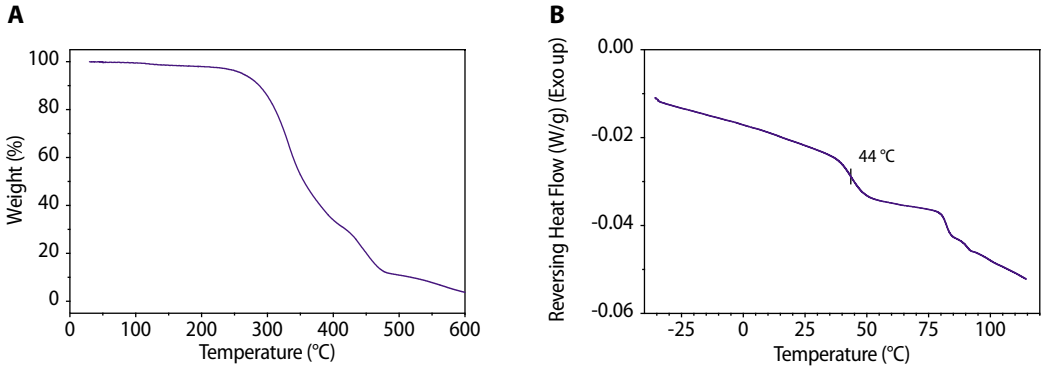

Figure S35 – (A) TGA and (B) mDSC curves for **P(HMDA75)-(PRI25)**.

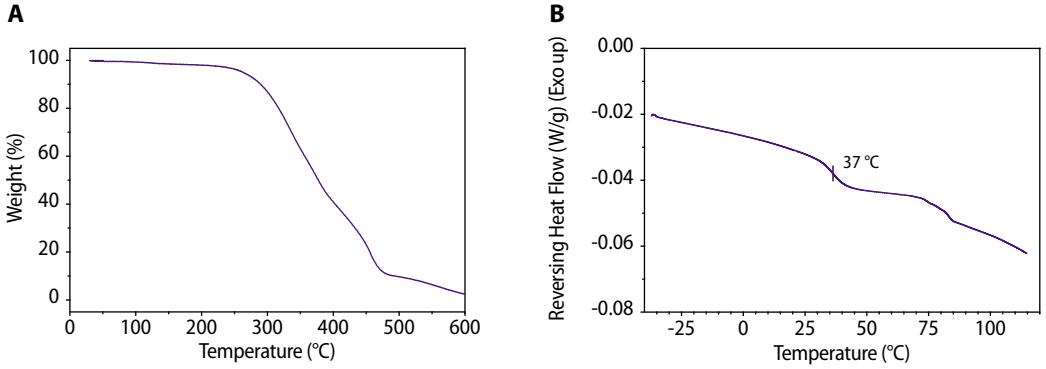

Figure S36 – (A) TGA and (B) mDSC curves for **P(HMDA50)-(PRI50)**.

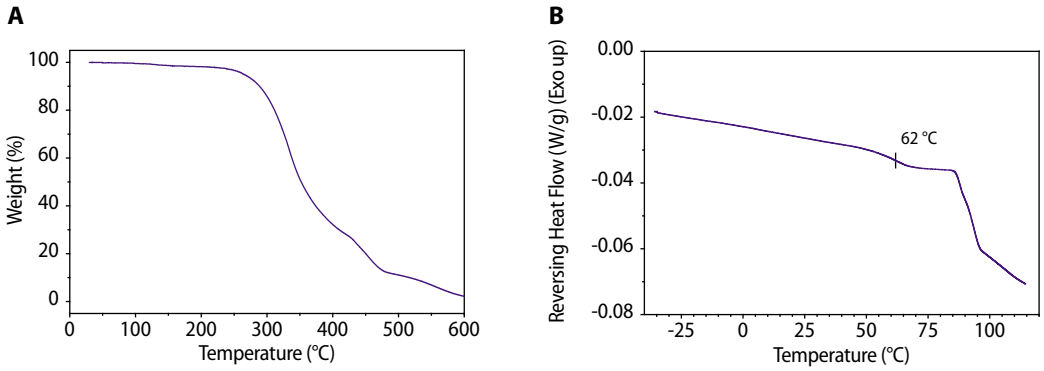

Figure S37 – (A) TGA and (B) mDSC curves for **P(XDA75)-(PRI25)**.

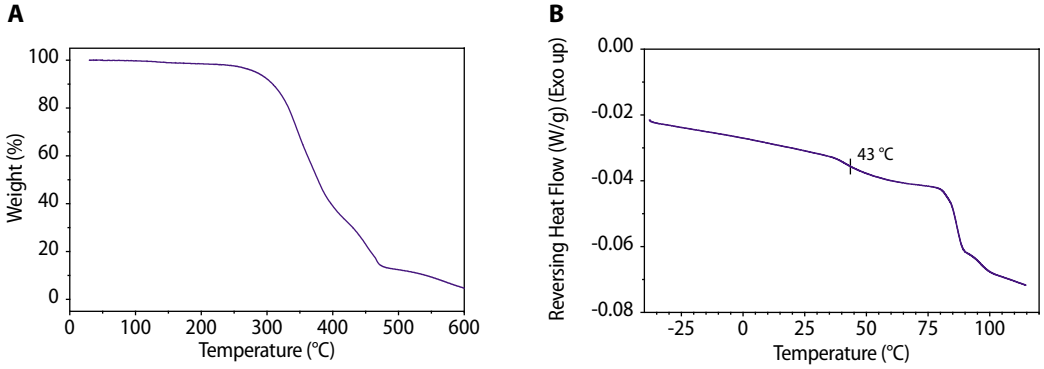

Figure S38 – (A) TGA and (B) mDSC curves for **P(XDA50)-(PRI50)**.

9. Dynamic Mechanical Analysis

DMTA was performed to observe the thermal behavior of a typical network, P-DMDO, in temperatures inaccessible with our rheology setup. A temperature ramp was therefore performed from room temperature to 80 °C. This maximum temperature limit was selected to avoid polymer flow which might damage the instrument. As the temperature increased, a drop in storage modulus was observed due to the glass transition of the polymer, which showed to be very similar (2 °C of difference) to the one determined by DSC analysis.

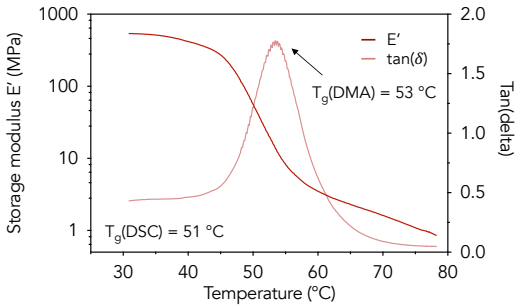

Figure S39 – Temperature ramp analysis by DMTA of P-DMDO, displaying a T_g very similar to the T_g determined by DSC.

10. Rheological data

Stress relaxation experiments were achieved at different temperatures for a given material. One- or two-element Maxwell and stretched exponential models didn't gave satisfactory results with low fitting accuracy. The data was then fitted to a three-element Maxwell model with which high values of R^2 could be obtained (typically $R^2 > 0.99$)

$$G(t) = G_0 + G_1 e^{-t/\tau_1} + G_2 e^{-t/\tau_2} + G_3 e^{-t/\tau_3}$$

Only the slowest relaxation time τ_3 showed a temperature-dependence behavior. An energy of activation could be determined from the slope of the linear fit in an Arrhenius plot following the equation:

$$\ln(\tau_3) = \ln(\tau_0) + \frac{E_a}{RT}$$

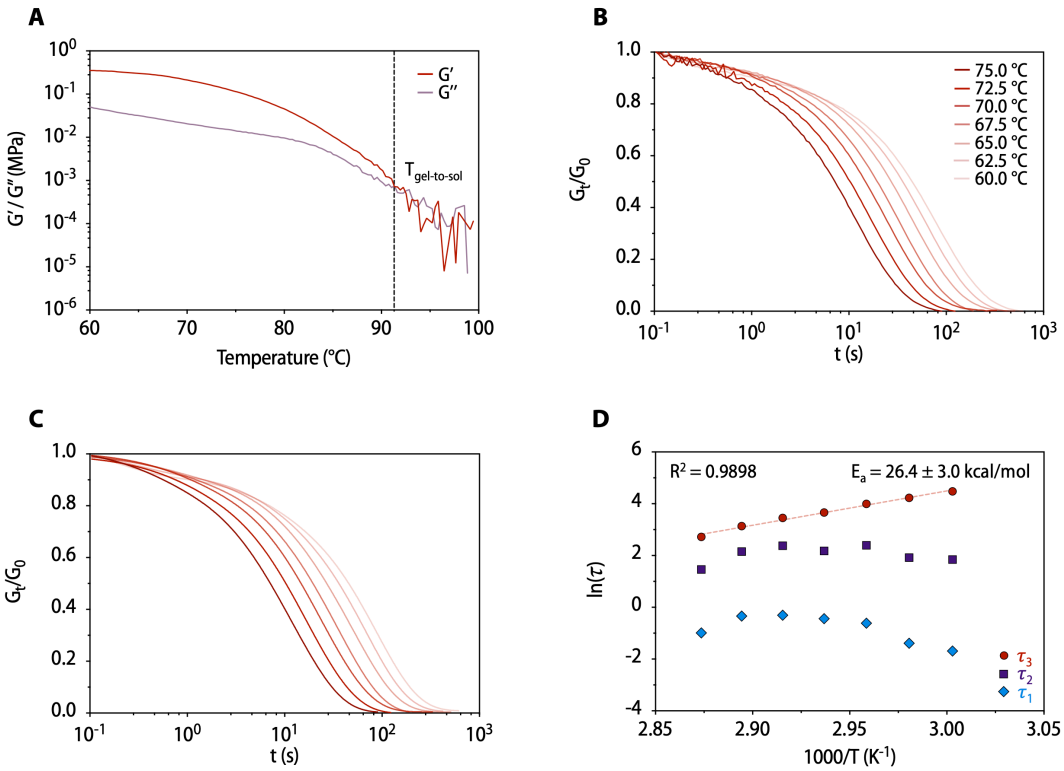

Figure S40 – For P-DMDO, different rheological experiments were conducted: (A) Temperature sweep, (B) Stress relaxation at different temperatures and (C) their respective curve fits. (D) The three relaxation times were plotted for each temperature, the third one used with the Arrhenius law to extract an energy of activation.

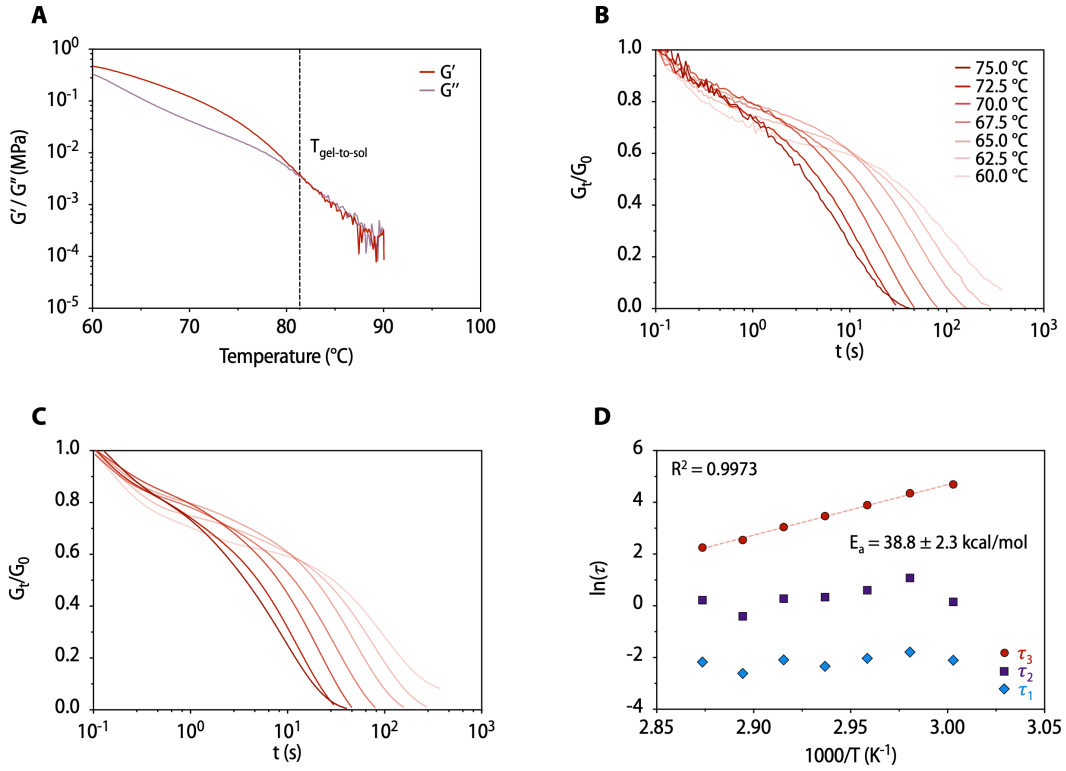

Figure S41 – For P-HMDA, different rheological experiments were conducted: (A) Temperature sweep, (B) Stress relaxation at different temperatures and (C) their respective curve fits. (D) The three relaxation times were plotted for each temperature, the third one used with the Arrhenius law to extract an energy of activation.

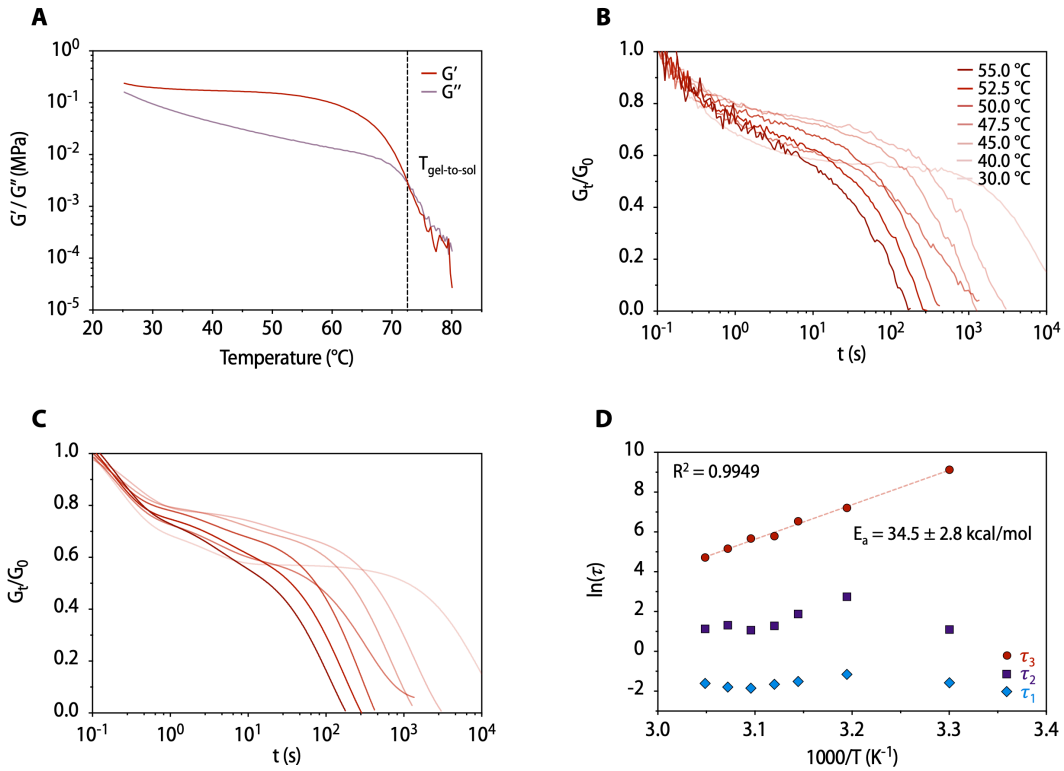

Figure S42 – For P-PRI, different rheological experiments were conducted: (A) Temperature sweep, (B) Stress relaxation at different temperatures and (C) their respective curve fits. (D) The three relaxation times were plotted for each temperature, the third one used with the Arrhenius law to extract an energy of activation.

Table S3 – From a fitting of the relaxation curve to the model, three relaxation times were determined at each temperature. The good fitting was highlighted by an excellent R^2 in all cases.

T (°C) DMDO	τ_1 (s)	τ_2 (s)	τ_3 (s)	R^2
60	0,1844	6,318	88,25	0.9999
62.5	0,2505	6,852	68,67	0.9999
65	0,5423	11	54,36	0.9999
67.5	0,6472	8,827	38,88	0.9999
70	0,7394	10,77	31,55	0.9999
72.5	0,7145	8,626	23,01	0.9995
75	0,3739	4,324	15,13	0.9998
T (°C) HMDA	τ_1 (s)	τ_2 (s)	τ_3 (s)	R^2
60	0,122	1,171	109,6	0.9995
62.5	0,1668	2,944	77,95	0.9996
65	0,1311	1,833	49,39	0.9998
67.5	0,09689	1,405	32,09	0.9996
70	0,124	1,318	21,05	0.9997
72.5	0,07337	0,6698	12,72	0.9994
75	0,1137	1,25	9,526	0.9986
T (°C) PRI	τ_1 (s)	τ_2 (s)	τ_3 (s)	R^2
30	0,2069	3,003	9239	0.9983
40	0,3147	15,58	1357	0.9980
45	0,222	6,537	688,6	0.9978
47,5	0,1927	3,598	328,8	0.9974
50	0,1578	2,92	290,7	0.9973
52,5	0,166	3,723	175,5	0.9963
55	0,2002	3,12	112,6	0.9886

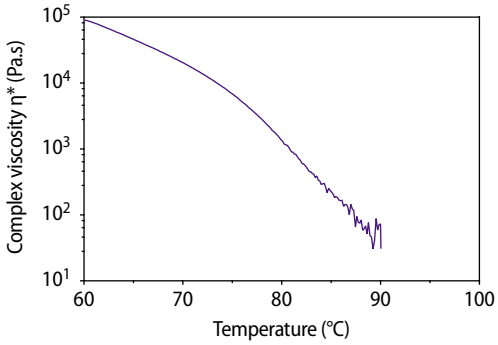

Figure S43 – Evolution of the complex viscosity of P-HMDA during a temperature sweep.

11. Polymer recycling

A. Mechanical recycling

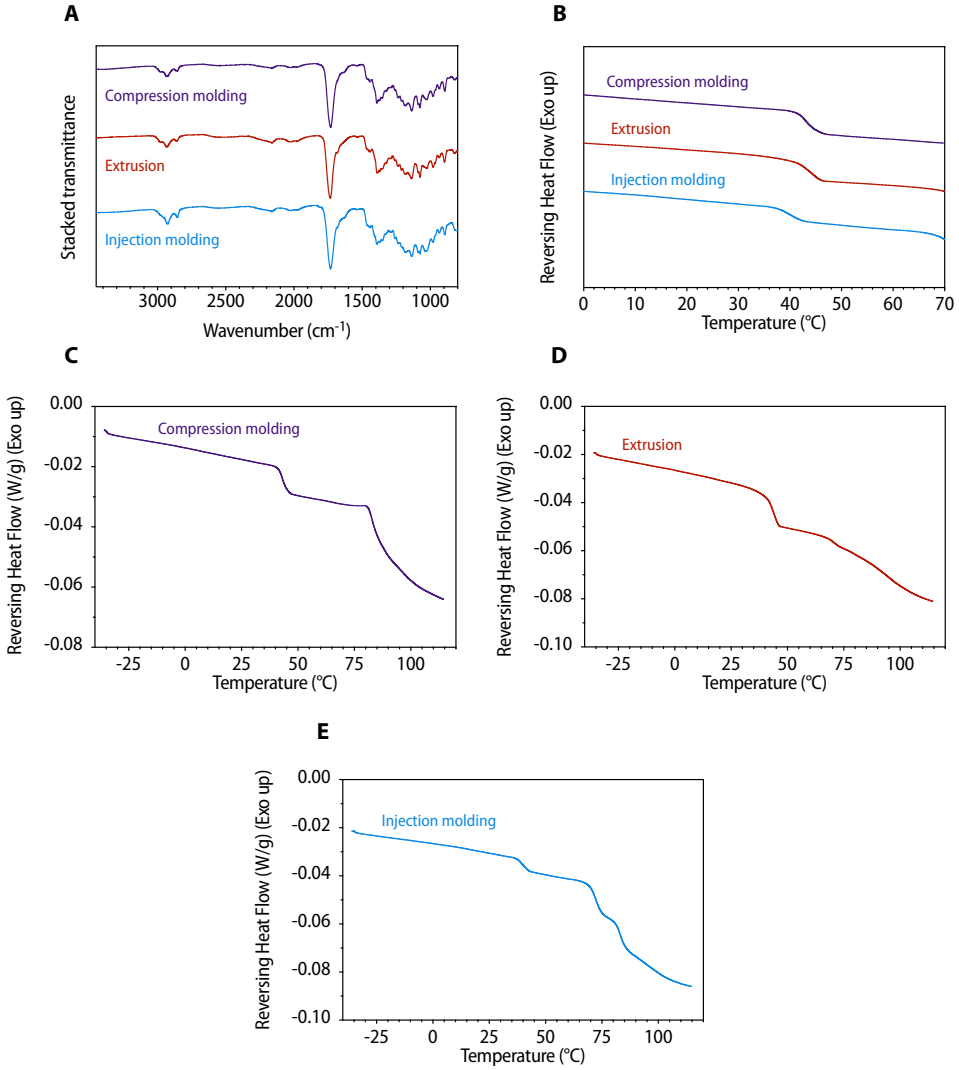

Figure S44 – (A) IR and (B) mDSC analyses of P-HMDA after mechanical recycling using various techniques. Complete DSC curves are provided in (C), (D) and (E). The endothermic phenomenon observed at around 75-80 °C in (C), (D) and (E) is attributed to dissociation within the polymer network.

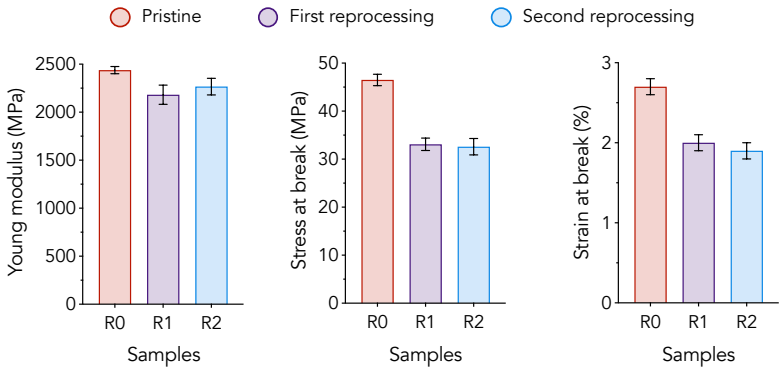

Figure S45 – Evolution of mechanical properties as determined by tensile tests after fracture and reprocessing of samples. R0 is the original material, R1 the material after one fracture and reprocessing, and R2 the material after two fractures and reprocessing.

B. Upcycling

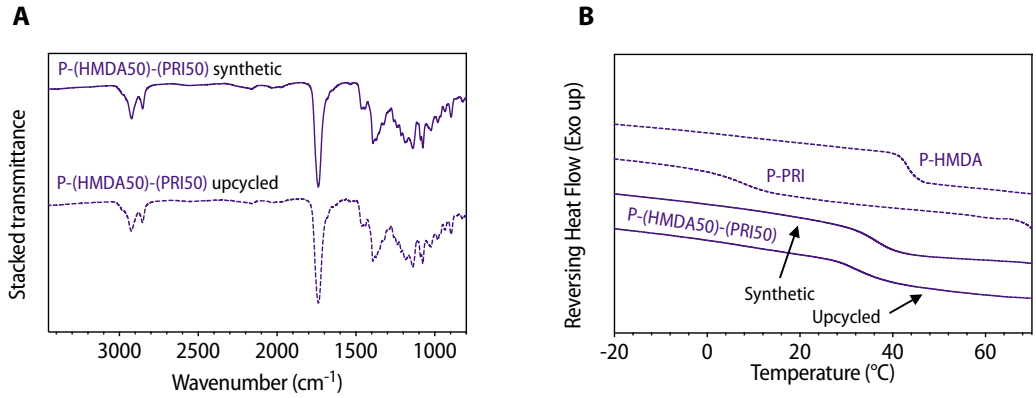

Figure S46 – (A) IR of synthetic and upcycled P-(HMDA50)-(PRI50). (B) mDSC analyses of P-HMDA, P-PRI, synthetic and upcycled P-(HMDA50)-(PRI50).

C. Chemical recycling

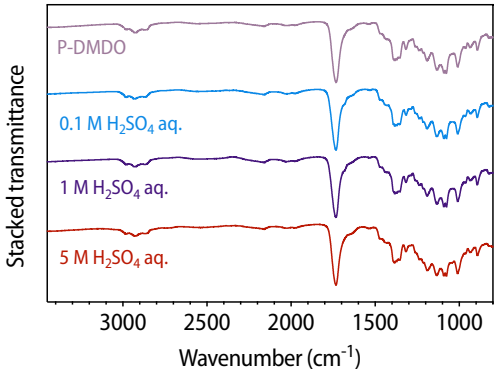

Figure S47 – After immersion of the polymer in H_2SO_4 aqueous solutions of different concentrations, the polymer was washed with water and dried under vacuum. The IR spectra show no difference after immersion in acidic water than the synthesized polymer.

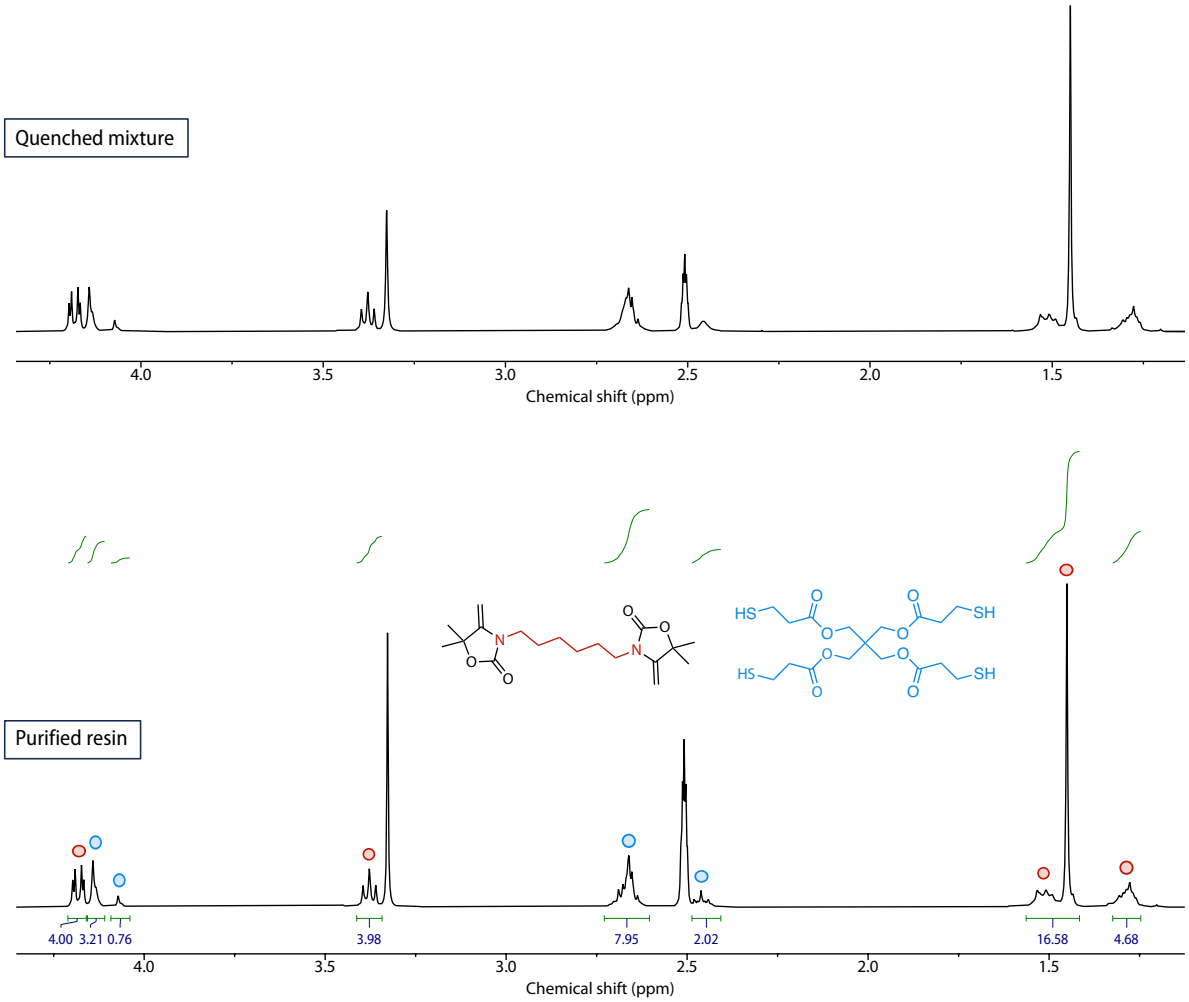

Figure S48 – ^{1}H-NMR spectrum (400 MHz, DMSO-d_6) of the **P-HMDA** resin after depolymerization and quench (top) and work-up (bottom). Integration of the signals shows the presence of the two compounds with functions in equimolar amounts.

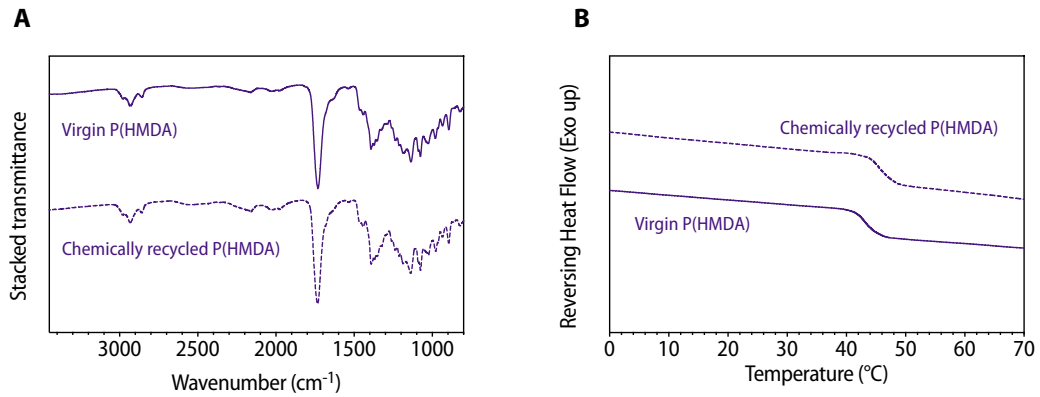

Figure S49 – (A) ATR-IR spectra and (B) mDSC curves of virgin P(HMDA) and the chemically recycled polymer.

12. Composite

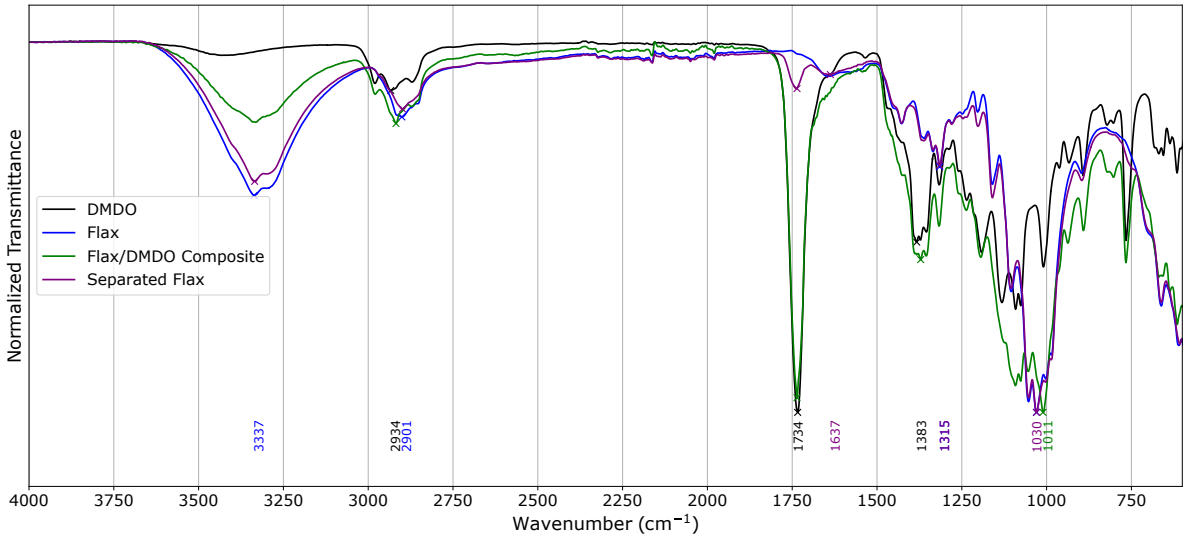

Figure S50 – Stacked ATR-IR spectra of P-DMDO polymer (black) and flax (blue). The Flax-DMDO composite (green) shows contribution of both constitutive components. The separated flax (purple) after dissolution of the polymer in $CHCl_3$ is very similar to the raw flax, with only very low contribution from P-DMDO as highlighted by the band at 1734 cm^{-1}.

13. Solvent resistance

The solvent resistance was assessed for a typical network (P-DMDO). To this aim, swelling ratios (SR) and gel contents (GC) were determined in solvents of very different nature: water as a polar and protic solvent, acetonitrile as a polar and aprotic solvent, THF as a solvent of medium polarity, and hexane as a solvent of low polarity. Table S4 showed that, except $CHCl_3$, all other solvents did not dissolve the polymer. Chloroform allowed for fast reaction kinetics and dissolution of the network (at rt, around 100 mg of P-DMDO in 30 mL of chloroform).

Table S4 – Swelling ratios and gel contents of P-DMDO in various solvents.

Solvent	H_2O	MeCN	THF	$CHCl_3$	Hexane
SR (%)	2.2 ± 0.1	90 ± 5	140 ± 4	soluble	1.1 ± 0.4
GC (%)	98.4 ± 0.4	89.3 ± 1.6	99.0 ± 0.3	soluble	99.8 ± 0.1

14. ωB97-XD/6-311++G(d,p) Optimized Cartesian Coordinates

Isolated reactants

Alkylidene oxazolidone

C	1.03672300	-0.98798500	-0.00005400
O	1.97203800	-1.74829300	0.00006600
O	-0.24537400	-1.38666800	-0.00002100
N	1.07998500	0.38315900	-0.00033800
C	-1.14648700	-0.24352100	0.00001900
C	-1.98632700	-0.31023400	-1.26642200
H	-2.58438500	-1.22389400	-1.27007500
H	-2.65835000	0.54939000	-1.30847800
H	-1.34814000	-0.29701700	-2.15195900
C	-1.98603000	-0.31003700	1.26665400
H	-2.65801200	0.54962200	1.30872100
H	-2.58413000	-1.22367100	1.27058900
H	-1.34766900	-0.29669500	2.15206300
C	-0.19065600	0.93715900	-0.00013700
C	2.30550600	1.14679600	0.00009400
H	2.35607600	1.77772600	0.89096600
H	3.14183600	0.45061500	0.00035700
H	2.35670300	1.77779800	-0.89068400
C	-0.49642300	2.23264400	-0.00006000
H	0.26736100	2.99962100	-0.00008900
H	-1.53233300	2.54514700	0.00003300

Methanethiol

S	-0.66203900	-0.08728200	0.00000000
H	-0.91208400	1.23195400	-0.00000500
C	1.15689200	0.01957300	0.00000100
H	1.52663600	-1.00529500	0.00002500
H	1.51836000	0.52618300	-0.89352000
H	1.51836000	0.52623500	0.89349100

MSA

C	1.63194000	0.29371600	-0.05204700
H	1.89550100	0.38004300	-1.10419600
H	2.18772700	-0.51446600	0.42174900
H	1.78985200	1.23163500	0.47673000
S	-0.08662500	-0.13515800	0.05658200
O	-0.34244900	-1.30275400	-0.75008100
O	-0.51197700	-0.09280300	1.43993200
O	-0.79938700	1.08530800	-0.72490000
H	-1.04820400	1.78501400	-0.10692300

Intermediates and transition states

Int1

C	-2.52525000	0.66299200	0.52306300
O	-2.95224500	1.73362800	0.86859600
O	-2.96053200	-0.00576600	-0.55249900

N	-1.54615500	-0.07926600	1.14851600
C	-2.26331200	-1.27331400	-0.69263100
C	-3.29037500	-2.39005200	-0.58001600
H	-4.02466900	-2.29892600	-1.38266200
H	-2.79346300	-3.35833100	-0.66693900
H	-3.80459300	-2.34607000	0.38189600
C	-1.53862900	-1.26753400	-2.02974600
H	-0.97701800	-2.19653400	-2.15027100
H	-2.26364000	-1.19135400	-2.84231400
H	-0.84908100	-0.42344100	-2.08759700
C	-1.30759300	-1.25932000	0.48748200
C	-0.85045300	0.35399200	2.34140100
H	0.22482300	0.38494600	2.15300000
H	-1.20809800	1.34924800	2.59797000
H	-1.05727000	-0.33112500	3.16710500
C	-0.41526000	-2.20192700	0.82073000
H	0.18303400	-2.12230900	1.72025000
H	-0.36075500	-3.11964500	0.24889900
H	1.00061300	-1.32348200	-0.34794300
C	-0.38549200	3.71238700	-0.20074600
H	-1.15029300	3.43095200	0.52114500
H	0.40690500	4.28716400	0.27605600
H	-0.84168000	4.31614700	-0.98462500
S	0.29226200	2.22927800	-1.01597500
H	0.84025000	1.66606300	0.07524500
S	2.94513400	-0.54992600	0.16565300
O	2.38088100	0.30875200	1.19645800
O	1.77343200	-0.96322100	-0.84594100
C	3.92632200	0.40764400	-0.95291600
H	3.32602400	1.24803400	-1.29786300
H	4.79095500	0.75096000	-0.38646200
H	4.23334100	-0.23296000	-1.77710500
O	3.66466700	-1.73255800	0.58938800

TS1

C	-2.52243500	0.63949600	0.50414900
O	-2.95923200	1.68946100	0.86638900
O	-2.94908700	-0.06668700	-0.53702500
N	-1.48031800	-0.08062500	1.12980300
C	-2.20832500	-1.30889300	-0.65786400
C	-3.18694200	-2.46331900	-0.48844100
H	-3.94081000	-2.41025200	-1.27515000
H	-2.65810000	-3.41377100	-0.57412700
H	-3.68130000	-2.41900100	0.48357900
C	-1.49207800	-1.31936900	-2.00052500
H	-0.90226400	-2.23238300	-2.09741500
H	-2.23265600	-1.29152800	-2.80104800
H	-0.82980900	-0.45782300	-2.09026300
C	-1.24023900	-1.22448100	0.49789100
C	-0.75894900	0.42399600	2.28918500
H	0.29809900	0.52951900	2.03857700
H	-1.18425100	1.39110300	2.54749300
H	-0.88397800	-0.26544500	3.12521800

C	-0.22448500	-2.12642800	0.78063400
H	0.20424000	-2.09411400	1.77867800
H	-0.33480000	-3.11740100	0.35124300
H	0.77473700	-1.60468300	0.03996500
C	-0.35202200	3.68668800	-0.11876900
H	-0.90655000	3.38994100	0.76981500
H	0.52746500	4.26738000	0.15479200
H	-0.99958900	4.29472100	-0.74946600
S	0.11961700	2.22681600	-1.10290700
H	0.94155400	1.66136000	-0.19501600
S	2.87859700	-0.50722200	0.14329000
O	2.31908400	0.55028700	1.00054200
O	1.75293400	-1.18622400	-0.64659900
C	3.82935000	0.27701800	-1.13870000
H	3.18650000	0.98667200	-1.65728300
H	4.65972500	0.79033000	-0.65550300
H	4.19408300	-0.49193400	-1.81714700
O	3.72320900	-1.48309500	0.82456000

Int2a

C	-2.36065700	0.76152600	0.51653300
O	-2.67986100	1.81686200	0.95232300
O	-2.83072700	0.14575800	-0.54979300
N	-1.39266400	-0.12611700	1.13685600
C	-2.24112400	-1.17104300	-0.69794100
C	-3.36288600	-2.20008300	-0.62798100
H	-4.05989000	-2.00757500	-1.44405800
H	-2.95767300	-3.20516100	-0.74872700
H	-3.89836800	-2.13938300	0.32080100
C	-1.44935300	-1.22075300	-2.00003300
H	-1.02721000	-2.21789000	-2.13321600
H	-2.12938700	-1.00990700	-2.82606500
H	-0.63488700	-0.49650200	-1.98993700
C	-1.32332400	-1.24174000	0.48841300
C	-0.63316500	0.27740900	2.31988100
H	0.42153800	0.35112000	2.04143600
H	-1.01826100	1.24397100	2.63508500
H	-0.78448800	-0.45706200	3.10963900
C	-0.46192100	-2.37637200	0.81248100
H	-0.11748000	-2.35630900	1.84447800
H	-0.96098200	-3.31761300	0.58293200
H	0.41332400	-2.27354300	0.14852200
C	-0.10967200	3.75085400	-0.05473500
H	-0.62021500	3.50436100	0.87511500
H	0.82262200	4.27433400	0.15215600
H	-0.75555200	4.39641100	-0.64907800
S	0.19858600	2.25121900	-1.04292300
H	1.03514900	1.63134200	-0.17925000
S	2.72702500	-0.60408300	0.06433600
O	2.23679500	0.46516500	0.97623600
O	1.68305400	-0.99856500	-0.91534600
C	4.04148700	0.14098500	-0.88943400
H	3.63030900	0.99514700	-1.42634700

H	4.82509700	0.45984900	-0.20357100
H	4.42366700	-0.60280300	-1.58719900
O	3.30764500	-1.75032600	0.78327800

Int2b

C	-2.23204700	0.83800700	0.90568600
O	-2.29258500	1.84197100	1.53269700
O	-3.07772000	0.39123300	-0.00363700
N	-1.18979600	-0.15821100	1.05810400
C	-2.66525600	-0.90397800	-0.50237100
C	-3.74646200	-1.91910000	-0.14462400
H	-4.67700700	-1.61537400	-0.62504000
H	-3.47125300	-2.90805600	-0.51263400
H	-3.90060200	-1.96733000	0.93436800
C	-2.40472800	-0.80280100	-2.00015300
H	-2.05754500	-1.76368000	-2.38246600
H	-3.33822300	-0.54255400	-2.50003300
H	-1.65772700	-0.03868000	-2.21411900
C	-1.39908400	-1.15792800	0.26570300
C	-0.09232800	0.07207600	1.99227400
H	0.52536800	-0.82003000	2.05547300
H	0.51858200	0.89159400	1.61481300
H	-0.51780400	0.33336200	2.95930200
C	-0.53850900	-2.32478500	0.08659300
H	-0.08513900	-2.64789300	1.02336700
H	-1.07402200	-3.14058600	-0.39377900
H	0.29264800	-1.98227100	-0.55542300
C	0.67429200	3.16723500	0.02958500
H	-0.02827500	3.22531800	0.86088700
H	1.59150900	2.67168200	0.34742500
H	0.90216700	4.17236500	-0.32210100
S	-0.06141400	2.20906300	-1.34458400
H	0.73732200	1.11781000	-1.25528100
S	2.79807600	-0.55691300	0.05574500
O	1.73977900	-0.58890200	-0.99628000
O	2.59008500	-1.60919300	1.07238300
C	4.32762900	-0.94750000	-0.78013500
H	4.23321600	-1.93538700	-1.22862100
H	4.50120500	-0.19288900	-1.54599400
H	5.12977400	-0.93652600	-0.04350000
O	2.96253500	0.79299700	0.63017500

TS2

C	2.38276300	1.50386300	0.48066300
O	2.41861200	2.57328400	1.00266300
O	3.31029200	0.55746500	0.55328600
N	1.32515500	1.01761000	-0.33820300
C	2.98695200	-0.54441900	-0.33328100
C	3.84028100	-0.39287900	-1.59951700
H	4.89048100	-0.39874100	-1.30740800
H	3.65902500	-1.23070900	-2.27426200
H	3.62427500	0.54094500	-2.12234100
C	3.28215500	-1.84794800	0.37929000

H	2.87655600	-2.68447600	-0.19216600
H	4.36299900	-1.97294500	0.45729400
H	2.84905200	-1.85747900	1.37696900
C	1.54451300	-0.23560400	-0.70255500
C	0.17608800	1.84321300	-0.69766300
H	-0.74539800	1.27940700	-0.55814300
H	0.17942000	2.71704000	-0.05064500
H	0.26369000	2.15409300	-1.73899600
C	0.83764800	-0.86815600	-1.84428900
H	1.24949400	-0.43350200	-2.76269300
H	1.01481600	-1.94254000	-1.86016800
H	-0.23417500	-0.66841900	-1.81265100
C	-0.16418400	-0.20895300	2.27706200
H	0.15220500	0.75833000	1.88193600
H	-1.23303600	-0.17201700	2.48494400
H	0.40176200	-0.43505300	3.17851600
S	0.13802900	-1.52909400	1.07122500
H	-0.96315900	-1.29216000	0.29178100
S	-3.33004400	0.10636100	-0.14016900
O	-2.26146700	-0.69634200	-0.81571400
O	-3.23182700	1.53782000	-0.47667400
C	-4.86988200	-0.48107600	-0.82955200
H	-4.85233500	-0.31308200	-1.90533100
H	-4.96415700	-1.54273100	-0.60637300
H	-5.68169200	0.08017700	-0.36876000
O	-3.37957000	-0.16646900	1.30869700

Int3

C	2.12500900	1.57209200	0.46925800
O	2.08696200	2.68416100	0.93695500
O	3.06315900	0.66316600	0.80145800
N	1.27441300	1.02505000	-0.44870000
C	2.97915500	-0.47299000	-0.10102200
C	3.97151400	-0.21071400	-1.23318400
H	4.96304400	-0.07510800	-0.79842100
H	4.01043200	-1.05697300	-1.92118100
H	3.71451400	0.69008700	-1.79413700
C	3.36489300	-1.72166200	0.66487000
H	3.21808900	-2.60216700	0.03545400
H	4.42033300	-1.66629800	0.93790800
H	2.77396800	-1.84422800	1.57104600
C	1.49366400	-0.39069200	-0.59090100
C	0.07828100	1.71727600	-0.88205000
H	-0.78087300	1.47211800	-0.25108400
H	0.26615200	2.78781900	-0.81953800
H	-0.14384600	1.45814500	-1.91756400
C	1.26829100	-0.91201100	-2.00501500
H	1.84080400	-0.32560700	-2.72343200
H	1.57914900	-1.95641600	-2.07528400
H	0.21419000	-0.85451700	-2.27965600
C	0.22392600	-0.45145700	2.01510100
H	-0.14164200	0.56003800	1.84395300
H	-0.49393500	-0.97663700	2.64480000

H	1.19479700	-0.43599700	2.50824500
S	0.29486100	-1.38362000	0.46324400
H	-1.60416900	-0.97577900	-0.41495900
S	-3.50544500	-0.07074900	0.09347200
O	-2.47208300	-0.80930700	-0.87498200
O	-2.75294200	0.75950100	1.01965000
C	-4.34120600	0.94350900	-1.09452400
H	-3.61745400	1.62876600	-1.53066500
H	-4.78187800	0.29520200	-1.84943200
H	-5.11560800	1.48547800	-0.55334200
O	-4.43119200	-1.04170400	0.63761000

Isolated product

C	-0.58746200	-1.47916700	-0.49383700
O	-1.31443500	-2.35137200	-0.90827100
O	0.56980300	-1.14011600	-1.09718100
N	-0.76535600	-0.69507800	0.60718400
C	1.32114600	-0.24134000	-0.23470200
C	2.26881800	-1.11566400	0.58643300
H	2.89789600	-1.68426200	-0.10051400
H	2.91505400	-0.50393100	1.21830500
H	1.72272800	-1.82006800	1.21722400
C	2.10755400	0.71660200	-1.10507300
H	2.61172800	1.45429700	-0.47678200
H	2.86637800	0.16226700	-1.66098700
H	1.47048500	1.24712500	-1.81008400
C	0.18815400	0.39090800	0.64145300
C	-1.98678300	-0.71219700	1.38171600
H	-2.56373500	-1.58578800	1.08372600
H	-1.76051300	-0.77938900	2.44731800
H	-2.57523500	0.19157300	1.19684700
C	0.62457300	0.76431400	2.05369100
H	-0.20247500	1.21664900	2.60276500
H	0.95838900	-0.11843600	2.59919500
H	1.44337100	1.48596200	2.01722700
S	-0.56015000	1.95993700	-0.04297700
C	-1.39644200	1.38911300	-1.54614900
H	-0.69551600	1.00336100	-2.28594800
H	-2.14497500	0.63092400	-1.31282300
H	-1.90398000	2.26276500	-1.95570300

15. References

(1) Song, Q.-W.; Chen, W.-Q.; Ma, R.; Yu, A.; Li, Q.-Y.; Chang, Y.; He, L.-N. Bifunctional Silver(I) Complex-Catalyzed CO_2 Conversion at Ambient Conditions: Synthesis of α-Methylene Cyclic Carbonates and Derivatives. *ChemSusChem* **2015**, *8* (5), 821–827. https://doi.org/10.1002/cssc.201402921.

(2) Stewart, J. J. P. Optimization of Parameters for Semiempirical Methods VI: More Modifications to the NDDO Approximations and Re-Optimization of Parameters. *J Mol Model* **2013**, *19* (1), 1–32. https://doi.org/10.1007/s00894-012-1667-x.

(3) James J. P. Stewart. MOPAC2016. http://openmopac.net.

(4) Frisch, M. J.; Trucks, G. W.; Schlegel, H. B.; Scuseria, G. E.; Robb, M. A.; Cheeseman, J. R.; Scalmani, G.; Barone, V.; Petersson, G. A.; Nakatsuji, H.; Li, X.; Caricato, M.; Marenich, A. V.; Bloino, J.; Janesko, B. G.; Gomperts, R.; Mennucci, B.; Hratchian, H. P.; Ortiz, J. V.; Izmaylov, A. F.; Sonnenberg, J. L.; Williams-Young, D.; Ding, F.; Lipparini, F.; Egidi, F.; Goings, J.; Peng, B.; Petrone, A.; Henderson, T.; Ranasinghe, D.; Zakrzewski, V. G.; Gao, J.; Rega, N.; Zheng, G.; Liang, W.; Hada, M.; Ehara, M.; Toyota, K.; Fukuda, R.; Hasegawa, J.; Ishida, M.; Nakajima, T.; Honda, Y.; Kitao, O.; Nakai, H.; Vreven, T.; Throssell, K.; Montgomery, J. A., Jr.; Peralta, J. E.; Ogliaro, F.; Bearpark, M. J.; Heyd, J. J.; Brothers, E. N.; Kudin, K. N.; Staroverov, V. N.; Keith, T. A.; Kobayashi, R.; Normand, J.; Raghavachari, K.; Rendell, A. P.; Burant, J. C.; Iyengar, S. S.; Tomasi, J.; Cossi, M.; Millam, J. M.; Klene, M.; Adamo, C.; Cammi, R.; Ochterski, J. W.; Martin, R. L.; Morokuma, K.; Farkas, O.; Foresman, J. B.; Fox, D. J. Gaussian 16, Revision C.01, 2016.

(5) Chai, J.-D.; Head-Gordon, M. Long-Range Corrected Hybrid Density Functionals with Damped Atom–Atom Dispersion Corrections. *Phys. Chem. Chem. Phys.* **2008**, *10* (44), 6615. https://doi.org/10.1039/b810189b.

(6) Logan, S. R. The Kinetics of Isotopic Exchange Reactions. *J. Chem. Educ.* **1990**, *67* (5), 371. https://doi.org/10.1021/ed067p371.

(7) Van Herck, N.; Maes, D.; Unal, K.; Guerre, M.; Winne, J. M.; Du Prez, F. E. Covalent Adaptable Networks with Tunable Exchange Rates Based on Reversible Thiol–Yne Cross-Linking. *Angew. Chem. Int. Ed.* **2020**, *59* (9), 3609–3617. https://doi.org/10.1002/anie.201912902.

(8) Denissen, W.; Rivero, G.; Nicolaÿ, R.; Leibler, L.; Winne, J. M.; Du Prez, F. E. Vinylogous Urethane Vitrimers. *Adv. Funct. Mater.* **2015**, *25* (16), 2451–2457. https://doi.org/10.1002/adfm.201404553.

(9) Haida, P.; Signorato, G.; Abetz, V. Blended Vinylogous Urethane/Urea Vitrimers Derived from Aromatic Alcohols. *Polym. Chem.* **2022**, *13* (7), 946–958. https://doi.org/10.1039/D1PY01237A.

(10) Christensen, P. R.; Scheuermann, A. M.; Loeffler, K. E.; Helms, B. A. Closed-Loop Recycling of Plastics Enabled by Dynamic Covalent Diketoenamine Bonds. *Nat. Chem.* **2019**, *11* (5), 442–448. https://doi.org/10.1038/s41557-019-0249-2.

(11) Röttger, M.; Domenech, T.; Van Der Weegen, R.; Breuillac, A.; Nicolaÿ, R.; Leibler, L. High-Performance Vitrimers from Commodity Thermoplastics through Dioxaborolane Metathesis. *Science* **2017**, *356* (6333), 62–65. https://doi.org/10.1126/science.aah5281.

(12) Delahaye, M.; Winne, J. M.; Du Prez, F. E. Internal Catalysis in Covalent Adaptable Networks: Phthalate Monoester Transesterification As a Versatile Dynamic Cross-Linking Chemistry. *J. Am. Chem. Soc.* **2019**, *141* (38), 15277–15287. https://doi.org/10.1021/jacs.9b07269.

(13) Houck, H. A.; De Bruycker, K.; Billiet, S.; Dhanis, B.; Goossens, H.; Catak, S.; Van Speybroeck, V.; Winne, J. M.; Du Prez, F. E. Design of a Thermally Controlled Sequence of Triazolinedione-Based Click and Transclick Reactions. *Chem. Sci.* **2017**, *8* (4), 3098–3108. https://doi.org/10.1039/C7SC00119C.

(14) Van Herck, N.; Du Prez, F. E. Fast Healing of Polyurethane Thermosets Using Reversible Triazolinedione Chemistry and Shape-Memory. *Macromolecules* **2018**, *51* (9), 3405–3414. https://doi.org/10.1021/acs.macromol.8b00368.